Environmental Science: Atmospheres

ROYAL SOCIETY OF CHEMISTRY

PAPER

View Article Online
View Journal

Cite this: DOI: 10.1039/d5ea00108k

Global modeling of trifluoroacetic acid surface concentration and deposition from the gas-phase oxidation of a wide range of precursor hydrofluoroolefins

M. Anwar H. Khan, [a] Danielle C. Mendes,[a] Rayne E. T. Holland, [a] Maria de los Angeles Garavagno,[a] Andrew J. Orr-Ewing, [a] Kieran M. Stanley, [a] Simon J. O'Doherty,[a] Dickon Young,[a] Martin K. Vollmer,[b] Alvin John Antony,[a] Fatima Karamshahi,[a] Timothy J. Wallington, [c] Carl J. Percival, [d] Asan Bacak,[ef] Richard G. Derwent[g] and Dudley E. Shallcross [*ah]

Oxidation of hydrofluoroolefins (HFOs) is a source of trifluoroacetic acid (TFA) in the lower atmosphere. TFA is deposited in precipitation and accumulates in water bodies and at land surfaces and concerns have been raised over its environmental impact. The formation and distribution of atmospheric TFA from the gas-phase oxidation of fifteen HFOs were studied. The deposition of TFA associated with regional emissions of HFOs were examined using a global three-dimensional chemical transport model, STOCHEM-CRI, where hypothetical scenarios with annual emissions of 1, 10 and 100 Gg for each of the HFOs were modelled. Globally, between 54 and 78 Gg year^{-1} of TFA are produced in scenarios using lower and upper limit TFA yields, respectively. The most significant contributors to the TFA formation are found to be HFO-1234yf (9.9 Gg year^{-1}, 13–18%), HFO-1225yeZ (8.5 Gg year^{-1}, 11–16%), HFO-1225yeE (8.6 Gg year^{-1}, 11–16%) and HFO-1216 (7.5 Gg year^{-1}, 10–14%). The tropospheric global burden and lifetime of TFA are found to be 0.54–0.78 Gg and 3.8 days, respectively. Atmospheric levels of TFA from HFO oxidation are highest in northern mid-latitudes, with up to 1.5–2.0 ppt in Europe, 0.5–0.7 ppt in Asia, and 0.5–0.7 ppt in North America during the northern hemispheric summer. TFA is mainly deposited in North America, Europe, and Asia, with deposition rates of up to 0.5 × 10^{-3} Mg km^{-2} years^{-1}, 1.0 × 10^{-3} Mg km^{-2} years^{-1}, and 1.0 × 10^{-3} Mg km^{-2} years^{-1}, respectively. A metric called the TFA deposition potential (TDP) is proposed that quantifies the extent to which different HFOs contribute towards enhanced environmental TFA deposition, relative to that from the oxidation of the most widely used HFO (HFO-1234yf).

Received 8th September 2025
Accepted 2nd December 2025

DOI: 10.1039/d5ea00108k

rsc.li/esatmospheres

Environmental significance

Oxidation of third and fourth generation refrigerants is likely to be a source of trifluoroacetic acid (TFA) which can be deposited in precipitation and accumulate in water bodies and at land surfaces, posing a risk to both aquatic and terrestrial ecosystems. As HFO use increases, the atmospheric levels of TFA and its environmental accumulation are anticipated to rise. In the study, we investigate the atmospheric formation and the surface deposition of TFA from fifteen candidate HFOs. We propose a metric called TFA deposition potential (TDP) which will be a useful tool to shape future policy development and industrial decisions concerning HFO use.

[a]School of Chemistry, University of Bristol, Cantock's Close, BS8 1TS, UK. E-mail: d.e.shallcross@bristol.ac.uk

[b]Laboratory for Air Pollution and Environmental Technology, Empa, Swiss Federal Laboratories for Materials Science and Technology, Dübendorf 8600, Switzerland

[c]Center for Sustainable Systems, School for Environment and Sustainability, University of Michigan, Ann Arbor, MI, 48109, USA

[d]Jet Propulsion Laboratory, California Institute of Technology, 4800 Oak Grove Dr, Pasadena, CA 91109, USA

[e]Ankara University Cancer Research Institute, Balkiraz Mahallesi, Mamak Caddesi No:1/8, 06620 Mamak, Ankara, Turkey

[f]Turkish Accelerator & Radiation Laboratory, Ankara University, 06830 Golbasi, Ankara, Turkey

[g]rdscientific, Newbury, RG14 6LH, UK

[h]Department of Chemistry, University of the Western Cape, Robert Sobukwe Road, Bellville 7305, South Africa

1 Introduction

Trifluoroacetic acid (TFA) is the simplest short-chain perfluoroalkyl acid (PFAA) and believed to be the most abundant of the wider class of persistent pollutants the per- and polyfluoroalkyl substances (PFAS).[1,2] Anthropogenic sources of TFA include the degradation of fluorinated refrigerants, pesticides and pharmaceuticals but the relative contributions of these different sources are unclear. The presence of significant levels of TFA in deep ocean water[3,4] suggests the presence of one, or more, natural sources.[5] Hydrofluoroolefins (HFOs) are an important class of fluorinated refrigerants and are an important contributor to atmospheric TFA formation and its subsequent deposition.[6]

The impacts of TFA on ecosystems are the topic of current debate. Research suggests that current and projected future TFA levels may be the cause of much concern for aquatic and terrestrial environments and for human health. For example, studies by Bott and Standley[7] saw a near 20-fold increase in ^{14}C labelled TFA in freshwater benthic microbial communities over a 2.5-year period compared with a control group, representing a small but statistically significant rate of incorporation. Zhang *et al.*[8] recorded high uptake levels of TFA in wheat compared with longer-chain PFAAs, and when TFA was exposed to sandy, low organic matter soil, Xu *et al.*[9] reported a decrease in soil pH (the soil became more acidic) and reduced bacterial abundance and soluble nutrients. Arp *et al.*[1] argue that TFA meets the three conditions of a planetary boundary threat, as defined by Persson *et al.*[10] In contrast, the UNEP Environmental Effects Assessment Panel find that with respect to the breakdown products of chemicals under the purview of the Montreal Protocol, the risks to ecosystem and human health from the formation of TFA as a degradation product of ozone depleting substances (ODS) replacements are currently de minimis. Madronich *et al.*[6] considered future emissions of HFO-1234yf out to 2100 and concluded that TFA was unlikely to have adverse ecosystem and human health impacts. Hanson *et al.* have reflected on the need for more data about TFA impacts in several areas, including its toxicology.[11]

Direct sources of TFA are unlikely, but atmospheric oxidation pathways of various PFAS precursors to TFA are likely to be important sources in the lower atmosphere.[1,2,10] Hydrofluorocarbons (HFCs) such as HFC-134a (CF_3CH_2F) can be oxidized to TFA *via* CF_3CFO hydrolysis,[12] and can lead to elevated TFA levels over terrestrial and aquatic surfaces.[13] However, the atmospheric lifetime of HFC-134a is long (*ca.* 14 years)[14] and so the enhanced surface concentrations of TFA are not very high. Hydrofluoroolefins (HFOs) such as HFO-1234yf (CF_3CFCH_2) tend to be much shorter lived, typically with atmospheric lifetimes of days to weeks.[14] Those HFOs that contain a CF_3-moiety can yield CF_3CFO or CF_3CHO on oxidation, which in turn can produce TFA (see SI, Fig. S1), which is likely to reach higher surface concentrations because the oxidation occurs close to emission sources.[15–17] Reports have noted high TFA levels in air and water close to fluorochemical emission sources,[18–20] and these studies suggest that breakdown of longer chain PFAS is also a significant source.[21] However, irrespective of the many potential sources of TFA, the emergence of HFOs as replacement compounds for the HFCs and HCFCs[22–24] present a significant new source of surface TFA in the environment owing to their short lifetimes and high yields of TFA upon oxidation. Indeed, interest in HFO oxidation is receiving greater attention because of the greater production not only of TFA, but also potentially of long-lived Greenhouse Gases (GHG) such as CF_3H.[25,26]

Recent gas-phase measurements of TFA in Toronto, Canada using I-CIMS showed levels up to 1.72 ppt in summer.[27] In this publication, authors speculated on sources of this TFA, and they noted that oxidation of HFO-1234yf can generate around 1 ppt, according to modelling studies, and may therefore be an important source.[13,28] There is a lack of data in the literature on the spatial distribution of TFA produced from the atmospheric degradation of HFOs. With increasing use of HFOs, and increasing interest in TFA, there is a need for studies of the atmospheric formation and the surface deposition of TFA from HFOs. Here, we report the results of global atmospheric modelling studies of the release and oxidation of fifteen candidate HFOs, as well as the associated TFA atmospheric concentrations and TFA deposition fluxes. We consider hypothetical scenarios with annual emissions of 1, 10 and 100 Gg for each of the HFOs (15, 150 and 1500 Gg year^{-1} total, respectively). The results for individual HFOs are reported separately and compared. The modelling methods follow those reported by Holland *et al.*[13,29] We also examine the TFA deposition on land and/or the oceans and we investigate how the surface TFA distribution arises from emissions in three regions (Europe, Asia and North America) as a function of HFO lifetime. The deposition fluxes reported here can be used with future emission estimates for individual HFOs to assess their contribution to TFA fluxes in the environment.

2 Materials and methods

A global three-dimensional chemical transport model, STOchastic CHEMistry – Common Representative Intermediates (STOCHEM-CRI), was used to simulate the emissions of HFOs, their oxidation and transportation of oxidation products such as TFA. In the STOCHEM-CRI model, the troposphere is split into 50 000 constant mass air parcels which are advected every three hours using a 4th order Runge–Kutta scheme *via* a Lagrangian approach.[30] It is an offline model with the transport and radiation driven by archived meteorological data from the UK Meteorological Office Unified Model which operates at a grid resolution of 1.25° longitude by 0.83° latitude and twelve unevenly spaced vertical levels, with an upper boundary up to 100 hPa.[31] The chemical and photochemical processes (*e.g.*, production and loss) that occur within the parcel, together with emission and physical loss (*e.g.*, deposition) are generally uncoupled from transport processes to enable local determination of the chemistry timestep.[32] The chemical mechanism in this model is the common representative intermediates mechanism (CRI v2.2). Details of the CRI v2 mechanism are given by Jenkin *et al.*,[33] Watson *et al.*,[34] and Utembe *et al.*,[35,36] with

Table 1 Kinetic data used in model simulations for the reaction of each HFO with OH radicals or ozone. Further explanation is provided in the SI

		Rate coefficients for the reaction of HFO + OH or O_3	
HFO	Formula	k_{OH} ($cm^3\ s^{-1}$)	k_{O_3} ($cm^3\ s^{-1}$)
HFO-1234yf	$CF_3CF{=}CH_2$	$1.26 \times 10^{-12} \exp(-35/T)$[38]	2.77×10^{-21} (296 K)[39]
HFO-1225yeZ	$CF_3CF{=}CHF$	$7.30 \times 10^{-13} \exp(165/T)$[38]	1.45×10^{-21} (296 K)[40]
HFO-1225yeE	$CF_3CF{=}CHF$	2.15×10^{-12} (296 K)[40]	1.98×10^{-20} (296 K)[40]
HCFO-1233zdZ	$CF_3CH{=}CHCl$	$7.22 \times 10^{-19}\ T^2 \exp(800/T)$[41]	1.53×10^{-21} (295 K)[42]
HCFO-1233zdE	$CF_3CH{=}CHCl$	$1.14 \times 10^{-12} \exp(-330/T)$[41]	1.46×10^{-21} (296 K)[43]
HFO-1234zeZ	$CF_3CH{=}CHF$	$9.11 \times 10^{-13} \exp(114/T)$[44]	1.65×10^{-21} (296 K)[45]
HFO-1234zeE	$CF_3CH{=}CHF$	$1.115 \times 10^{-13} (T/298)^{2.03} \exp(552/T)$[46]	2.81×10^{-21} (296 K)[47]
HFO-1336mzzZ	$CF_3CH{=}CHCF_3$	$5.73 \times 10^{-19}\ T^2 \exp(678/T)$[48]	6.25×10^{-22} (296 K)[49]
HFO-1336mzzE[a]	$CF_3CH{=}CHCF_3$	$6.94 \times 10^{-13} \exp(-496/T)$[50] $4.80 \times 10^{-13} \exp(-445/T)$[51]	4.14×10^{-22} (296 K)[49]
HFO-1318myZ	$CF_3CF{=}CFCF_3$	$2.99 \times 10^{-14} (T/298)^{2.61} \exp(760/T)$[52]	No data
HFO-1318myE	$CF_3CF{=}CFCF_3$	$7.50 \times 10^{-14} (T/298)^{1.68} \exp(612/T)$[52]	No data
HFO-1243zf	$CF_3CH{=}CH_2$	$7.65 \times 10^{-13} \exp(165/T)$[53]	3.01×10^{-19} (296 K)[54]
HFO-1438ezyE	$(CF_3)_2CFCH{=}CHF$	$7.34 \times 10^{-19}\ T^2 \exp(-481/T)$[55]	No data
HCFO-1233xf[a]	$CF_3CCl{=}CH_2$	2.39×10^{-12} (ref. 56) $9.43 \times 10^{-13} \exp(98/T)$[a][58]	3.5×10^{-21} (296 K)[57]
HFO-1216[a]	$CF_3CF{=}CF_2$	$9.75 \times 10^{-14} (T/298)^{1.94} \exp(922/T)$[52] $8.74 \times 10^{-13} \exp(260/T)$[59]	6.2×10^{-22} 296 K (ref. 60)

[a] Notes: the model was integrated with each choice of rate coefficient and the model outputs were compared, T is the atmospheric temperature in K.

updates in CRI v2.2 highlighted by Jenkin *et al.*[37] The chemistry scheme employs a backwards Euler solver with a five-minute timestep to evaluate an accurate solution to chemical ordinary differential equations.[33]

Wet deposition and dry deposition are the physical loss processes to remove TFA from air parcels particularly in the boundary layer. Whether a Lagrangian air parcel is treated as being above land or the ocean affects the rate of dry deposition because of the variability of the species deposition velocities. Wet deposition loss rates in STOCHEM combine species-dependent scavenging coefficients with scavenging profiles and precipitation rates. The dry deposition parameter of TFA (deposition velocity of TFA over land and sea of 1.9 mm s^{-1}), and wet deposition parameters of TFA (dynamic scavenging coefficient of 1.9 cm^{-1}, and convective scavenging coefficient of 3.8 cm^{-1}) are used in the model as reported by Holland *et al.*[13]

The emissions of 15 HFOs (1, 10 and 100 Gg $year^{-1}$ per HFO) from anthropogenic sources (industrial process and product use) were distributed using an annual source map of HFC-134a for the year 2010 at a resolution of 5° longitude by 5° latitude extracted from EDGARv4.2 with a resolution of 0.1° longitude by 0.1° latitude (http://edgar.jrc.ec.europa.eu/). An improved distribution over China in the EDGAR emission inventory was implemented, as described by Holland *et al.*[13] The emission totals of the other species (*e.g.*, VOCs, CO, and NO_x) employed in STOCHEM were taken from the Precursor of Ozone and their Effects in the Troposphere (POET) inventory (http://accent.aero.jussieu.fr/database_table_inventories.php). More details of the STOCHEM emissions inventory for all species can be found in Utembe *et al.*[36] In this study, the emissions of 15 HFOs, and their oxidation by OH and ozone, with rate coefficients summarized in Table 1, were incorporated into the STOCHEM-CRI model. The reported yields of TFA from OH initiated oxidation of different HFOs are summarized in SI (Table S1) which are used in the model simulations. TFA yield from O_3 initiated oxidation is assumed to be 0.95 for all HFOs as there are no reported values available. A couple of model simulations, STOCH-HFO-HY and STOCH-HFO-LY were performed using the higher and lower limits of TFA yields from the oxidation of HFOs, respectively (Table S1).

A couple of sensitivity experiments were conducted by changing the emission of individual HFO to 1 Gg $year^{-1}$ (total 15 Gg $year^{-1}$) in the runs hereafter referred to as STOCH-HFO-HY-1, STOCH-HFO-LY-1 and 100 Gr $year^{-1}$ (total 1500 Gg $year^{-1}$) in the runs hereafter referred to as STOCH-HFO-HY-100, STOCH-HFO-LY-100. We performed 15 and 8 additional simulations with STOCH-HFO-HY and STOCH-HFO-LY, respectively but addressing each individual HFO with emission of 10 Gg $year^{-1}$ (Table S2). A further nine simulations were performed, using the STOCH-HFO-HY formulation, to investigate regional impacts on TFA. Here, three HFOs the shortest lived HFO-1216 (5.3 days),[52] most widely used HFO1234yf of lifetime 12 days[38] and the longest lived HFO-1336mzzE (105 days)[51] were each emitted separately (with emissions derived from the global emissions of HFOs and following the EDGAR HFC-134a emissions distribution, as above) from North America (2.7 Gg $year^{-1}$), Europe (4.0 Gg $year^{-1}$) and Asia (2.7 Gg $year^{-1}$) to assess the impact. The basic features of all simulations and the differences between them can be found in SI Table S2. All simulations were conducted with meteorology from 1998 for a period of 24 months, with the first 12 months allowing the model to spin up. Analyses were performed on the subsequent 12 months of data.

3 Results and discussion

3.1 Selection of HFO emission inventory and their lifetimes

Selection of an appropriate HFO emission inventory to use in the model is important but challenging given the lack of

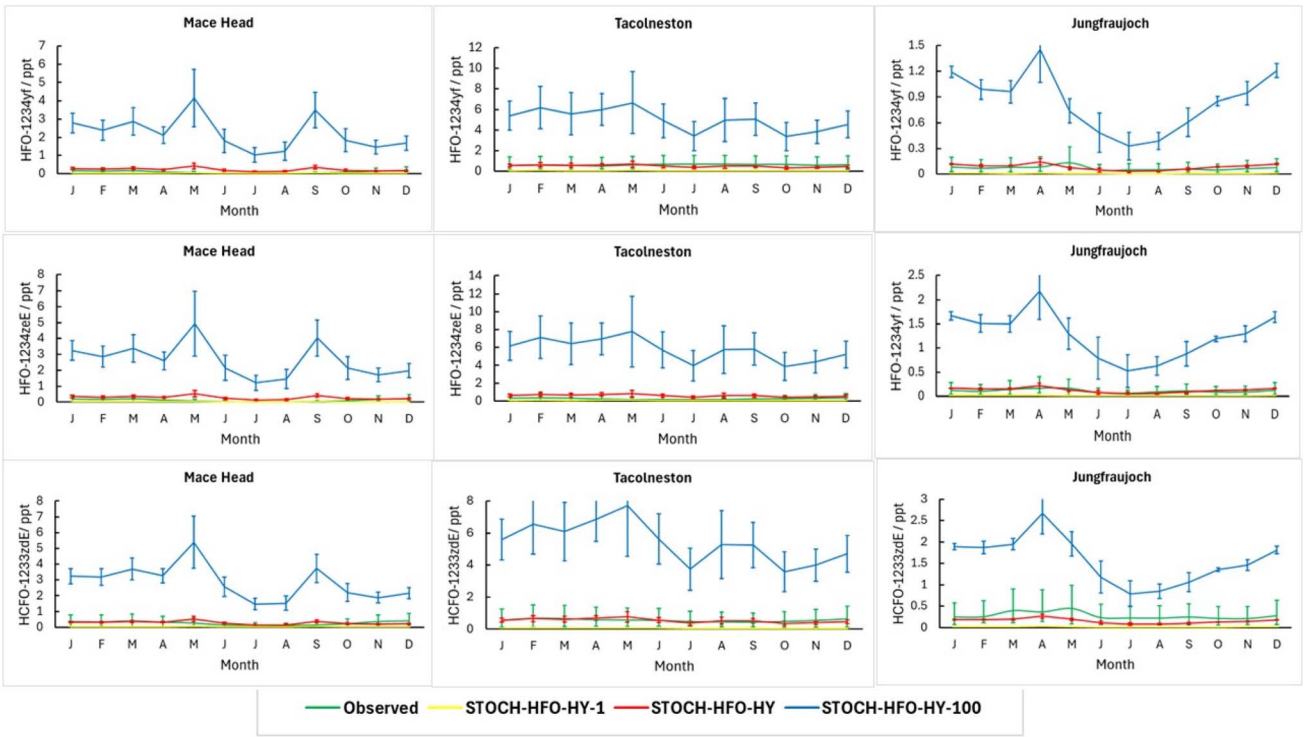

Fig. 1 Comparison of AGAGE (Mace Head, Tacolneston, Jungfraujoch) measurement data for HFO-1234yf, HFO-1234zeE and HCFO-1233zdE from Jan–Dec 2024 with the model data simulated by the STOCH-HFO-HY, STOCH-HFO-HY-1 and STOCH-HFO-HY-100. Green error bars represent measurement uncertainty. Yellow, red and blue error bars represent model uncertainty based on errors in sources and sinks in the model simulations with 1 Gg, 10 Gg and 100 Gg emissions of HFOs, respectively.

reported data. We used 1, 10 and 100 Gg year^{-1} for the emission of each individual HFO, giving a total of 15, 150 and 1500 Gg year^{-1} in this study. This is not to suggest that these emissions are an accurate representation of the current situation or a prediction of emissions in the future. A comparison of modelled HFO mixing ratios with measurement data from AGAGE (Advanced Global Atmospheric Gases Experiment, Jan–Dec 2024) stations shows that the modelled HFO-1234yf, HFO-1234zeE and HCFO-1233zdE mixing ratios are consistent with measurements at Mace Head, Tacolneston and Jungfraujoch (Fig. 1), when considering the 10 Gg year^{-1} HFO emission scenario. Average biases (model – measurement) of 0.008, 0.130, and −0.040 ppt for HFO-1234yf, HFO-1234zeE and HCFO-1233zdE, respectively, are calculated. Conversely, the biases are relatively high (−0.23 ppt for HFO-1234yf, −0.15 ppt for HFO-1234zeE, and −0.34 ppt for HCFO-1233zdE) for the emission scenario of 1 Gg and (2.43 ppt for HFO-1234yf, 3.05 ppt for HFO-1234zeE, and 2.91 ppt for HCFO-1233zdE) for the emission scenario of 100 Gg year^{-1}. All this suggests that the 10 Gg year^{-1} emission scenario is appropriate for the purposes of this study. There are no measurement data available for the other twelve HFOs, so we could not further validate the emissions inventory. Using the same emissions for all HFOs facilitates a comparison of their potential to produce TFA, thus providing valuable insights for future policy making.

There are no available kinetic data for the ozonolysis reactions of three of the 15 HFOs (HFO-1318myE, HFO-1318myZ, HFO-1438ezyE) (Table 1), so only OH oxidation is included in the model. The average comparative loss fluxes of the remaining twelve HFOs by OH and O_3 in the model show that ∼97% of HFOs loss is attributed to tropospheric OH, with a minor contribution from the ozonolysis reaction (∼3%). Except for HCFO-1233xf, all HFO lifetimes derived from the model are in close agreement with the reported WMO lifetimes (Table 2).[14] There is a large discrepancy between the lifetime of HCFO-1233xf calculated here and that reported by the WMO due to the use of different rate coefficients for the reaction with OH (k_{OH}) utilised. The k_{OH} used in this modelling study was derived using the theoretical methods.[56] The WMO panel,[14] following the JPL recommendations,[61] preferred to recommend a smaller value of k_{OH} (that of HCFO-1233xf) than that estimated by the theoretical study,[56] leading to an estimated lifetime of around 42 days. Thomsen and Jørgensen[56] instead estimated a lifetime for HCFO-1233xf of 5 days which is close to our study (7 days). For HFO-1336mzzE, HCFO-1233xf and HFO-1216, alternate reported k_{OH} values (as presented in Table 1) were considered. All alternate k_{OH} values (reported by Qing *et al.*,[51] Michelat *et al.*[58] and Tokuhashi *et al.*,[60] respectively) resulted in longer lifetimes, in better agreement with reported WMO values (Table 2). As a result, these k_{OH} values were carried through for use in subsequent simulations. Among the fifteen HFOs, the model predicts that HFO-1336mzzE and HFO-1216 are the longest and shortest lived HFOs, respectively.

Table 2 Tropospheric lifetimes of HFOs for reactions with OH and ozone, and comparisons with values from the WMO report[14]

HFO	Lifetime due to reaction with OH (days)	Lifetime due to reaction with O_3 (days)	Tropospheric total lifetime (days)	Total lifetime reported by WMO (days)
HFO-1234yf	13	6500	13	12
HFO-1225yeZ	11	12000	11	10
HFO-1225yeE	7	930	7	6
HCFO-1233zdZ	14	11800	14	13
HCFO-1233zdE	36	12300	36	42
HFO-1234zeZ	11	11000	11	10
HFO-1234zeE	19	6300	19	19
HFO-1336mzzZ	25	28600	25	27
HFO-1336mzzE	91	44600	91	120
	108[a]	45100[a]	108[a]	
HFO-1318myZ	31	—	31	n/a
HFO-1318myE	21	—	21	n/a
HFO-1243zf	10	60	8	9
HFO-1438ezyE	37	—	37	43
HCFO-1233xf	7	5300	7	42
	11[a]	5000[a]	11[a]	
HFO-1216	6	30000	6	n/a
	7[a]	30000[a]	7[a]	

[a] n/a represents no available literature data, calculated lifetime from the simulation using kinetic data from Qing *et al.*,[51] Michelat *et al.*[58] and Tokuhashi *et al.*[60] for the reaction of HFO-1336mzzmE + OH, HCFO-1233xf + OH, and HFO-1216 + OH, respectively.

3.2 TFA production from 15 HFOs and TFA loss processes

The model simulation results show that OH-initiated oxidation of all 15 HFOs produces most of the TFA (77.8 Gg year^{-1} (98%) for STOCH-HFO-HY and 53.9 Gg year^{-1} (97%) for STOCH-HFO-LY). Only the ozonolysis of HFO-1243zf produces a non-negligible amount of TFA (1.6 Gg year^{-1}). In combination, O_3-initiated oxidation of the other 11 HFOs produces only 0.2 Gg year^{-1} of TFA (Table 3). TFA production from the ozonolysis reactions of HFO-1318myE, HFO-1318myZ, HFO-1438ezyE could not be reported because of a lack of kinetic data. The yields of TFA from ozonolysis of HFOs depend on the specific HFO.[25] Therefore, using the same yield (0.95) for all twelve HFO ozonolysis reactions in the model may overestimate TFA production *via* this route. However, the fraction of TFA production from the ozonolysis reaction is much smaller than the production through OH-initiated HFO oxidation, thus using the same yield of TFA for all 12 HFOs ozonolysis reactions is unlikely to have a significant impact on the overall TFA formation in the model. The elevated levels of TFA formation from different HFOs vary depending on the HFO lifetimes. The oxidation of HFO-1234yf (9.9 Gg year^{-1}, 13–18%), HFO-1225yeZ (8.5 Gg year^{-1}, 11–16%), HFO-1225yeE (8.6 Gg year^{-1}, 11–16%) and HFO-1216 (7.5 Gg year^{-1}, 10–14%) have the largest contributions to TFA formation (Table 3 and Fig. 2). In Table 3, we

Table 3 TFA production fluxes from the oxidation of HFOs by OH and ozone and their contribution to total TFA production from the STOCH-HFO-HY and the STOCH-HFO-LY[a]

	Production of TFA (Gg year^{-1})		
HFO	OH oxidation	Ozonolysis	(TFA production by HFO)/(TFA production by HFO-1234yf)
HFO-1234yf	9.9	0.020	1.00
HFO-1225yeZ	8.5	0.007	0.86
HFO-1225yeE	8.5	0.065	0.87
HCFO-1233zdZ	2.6 (0.2)	0.010	0.26 (0.02)
HCFO-1233zdE	2.6 (0.2)	0.025	0.26 (0.02)
HFO-1234zeZ	3.3 (0.2)	0.011	0.34 (0.02)
HFO-1234zeE	3.3 (0.2)	0.033	0.34 (0.02)
HFO-1336mzzZ	4.1 (0.3)	0.006	0.42 (0.03)
HFO-1336mzzE	4.1 (0.3)	0.016	0.42 (0.03)
HFO-1318myZ	5.6	n/e	0.57
HFO-1318myE	5.6	n/e	0.57
HFO-1243zf	3.0 (0.2)	1.584	0.47 (0.18)
HFO-1438ezyE	4.8	n/e	0.48
HCFO-1233xf	2.6 (0.2)	0.018	0.26 (0.02)
HFO-1216	7.5	0.002	0.76

[a] n/e represents no estimate was made due to the unavailability of the kinetic data for ozonolysis reaction. The values are in brackets are produced from the model simulation, STOCH-HFO-LY.

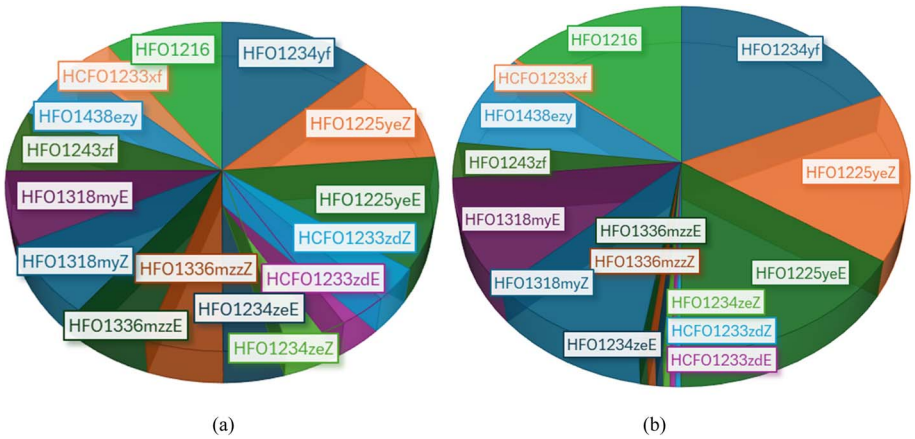

Fig. 2 Contribution of HFOs to atmospheric TFA formation flux derived from the model simulation, (a) STOCH-HFO-HY, (b) STOCH-HFO-LY.

compare relative TFA production from all HFOs with the most commonly used HFO, HFO-1234yf. HCFO-1233zdE, HCFO-1233zdZ, HFO-1333xf, HFO-1234zeZ and HFO-1234zeE contribute significantly less (0.70 and 0.98 times lower than that of HFO-1234yf in STOCH-HFO-HY and STOCH-HFO-LY, respectively) to the total TFA production. In terms of HFOs reactivity and the enhanced formation of TFA in STOCH-HFO-HY (Table 3), HFOs can be ranked as follows: HFO-1234yf > HFO-1225yeE ≈ HFO-1225yeZ > HFO-1216 > HFO-1318myZ > HFO-1318myE > HFO-1438ezyE > HFO-1243zf > HFO-

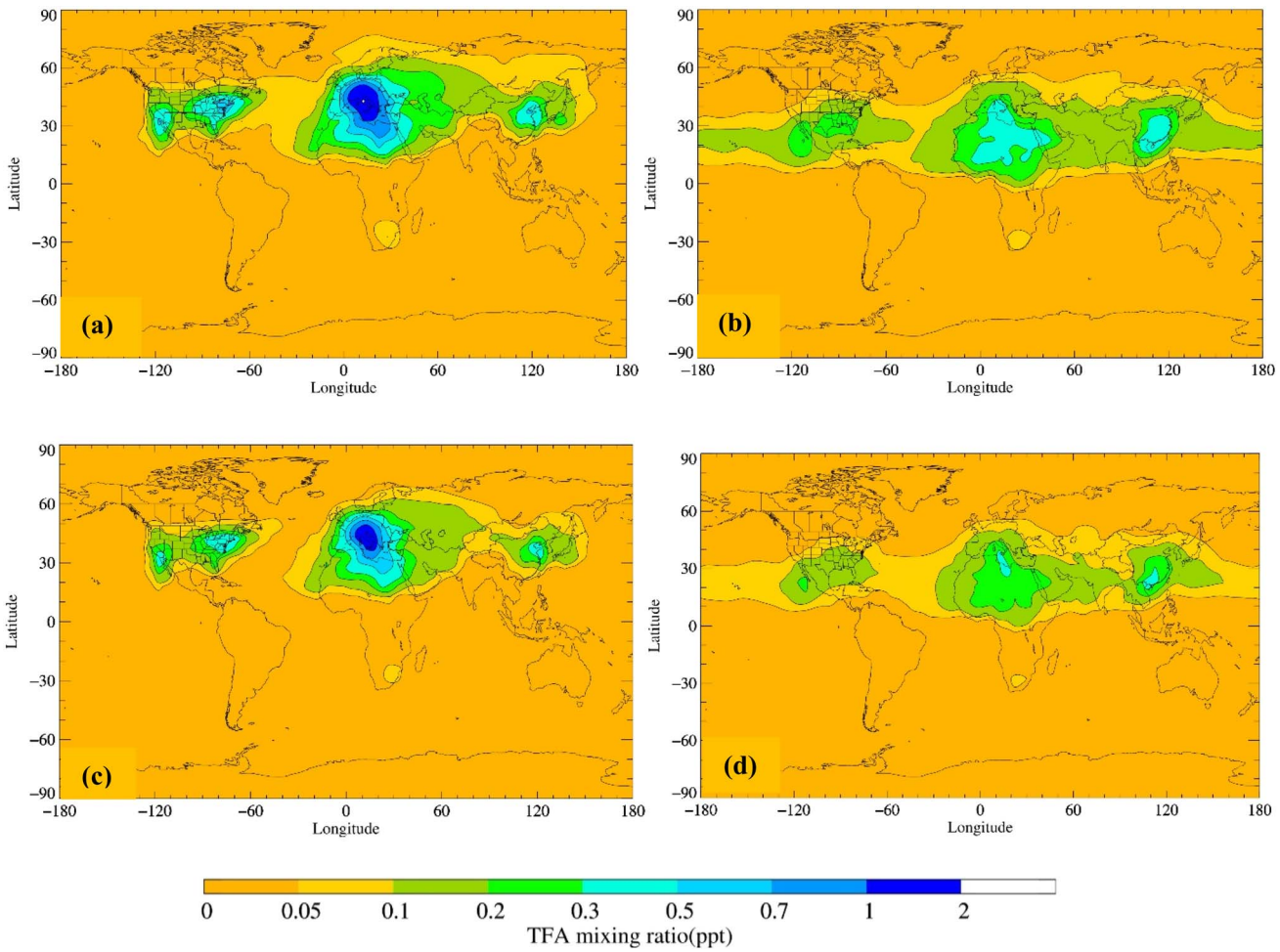

Fig. 3 Surface distributions of TFA simulated for (a) June-July-August, (b) December-January-February by the STOCH-HFO-HY model, and for (c) June-July-August, (d) December-January-February by the STOCH-HFO-LY model.

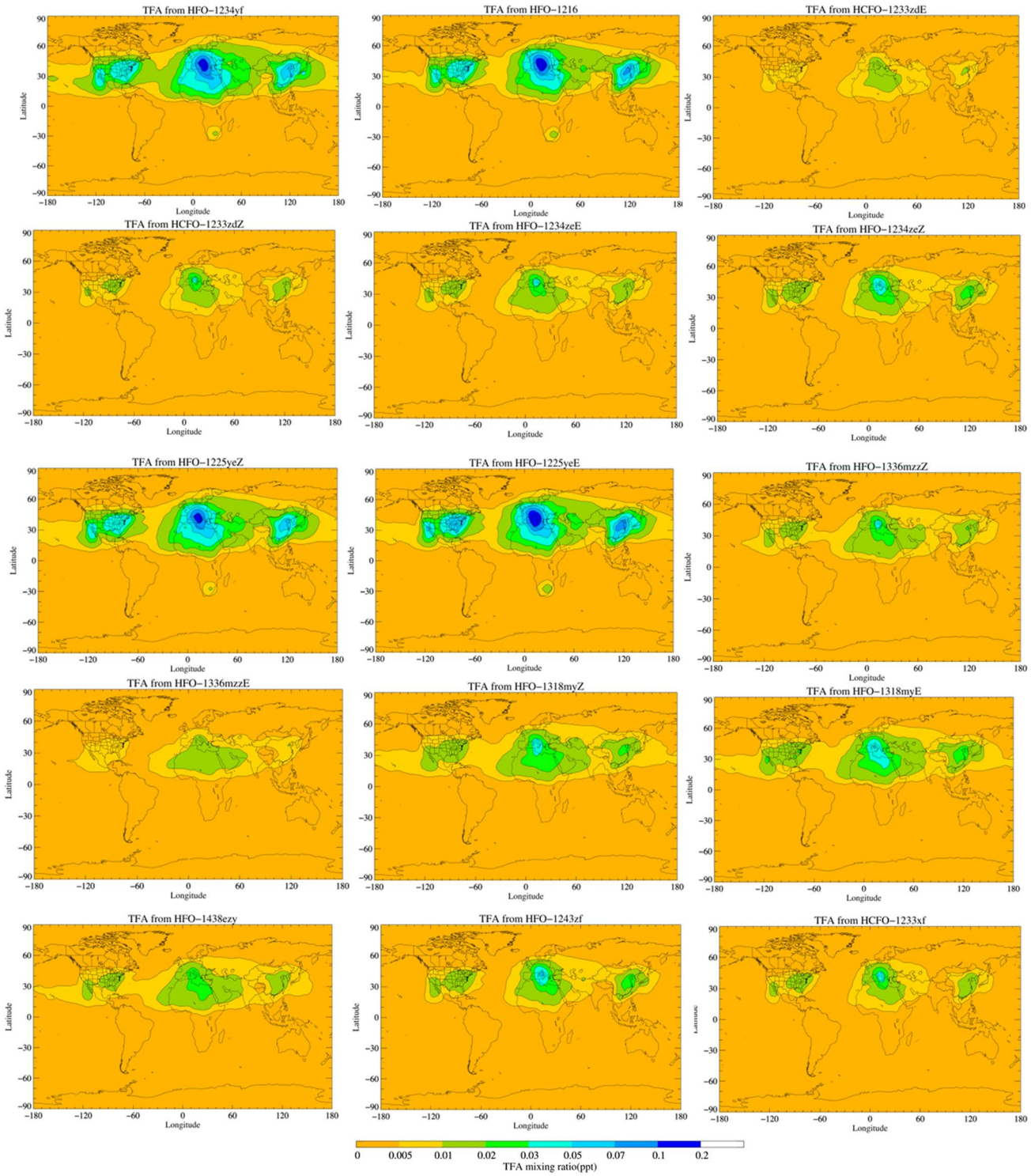

Fig. 4 Annual surface distribution plots of TFA mixing ratios produced from individual HFOs with higher TFA yields. The annual surface distribution plots of TFA mixing ratios produced from eight HFOs with lower TFA yields can be found in the SI (Fig. S4).

1336mzzmZ ≈ HFO-1336mzzE > HFO-1234zeZ ≈ HFO-1234zeE > HCFO-1233zdZ ≈ HCFO-1233zdE ≈ HCFO-1233xf. The ranking is consistent in STOCH-HFO-LY.

Wet deposition is the most significant atmospheric loss process for TFA (64.4 and 44.6 Gg year^{-1} (83%)), followed by dry deposition (8.5 and 5.9 Gg year^{-1} (11%)) and reaction with OH (4.8 Gg year^{-1} and 3.3 Gg year^{-1} (6%)) in STOCH-HFO-HY and STOCH-HFO-LY, respectively. This ordering agrees with the existing literature, which suggests that wet deposition is more important than dry deposition, while the gas-phase reaction of

TFA with OH is of minor significance.[17,28,62,63] The loss of TFA by reaction with stabilized Criegee intermediates was not included in the study as globally this loss process is insignificant compared with other loss processes.[13] The global burden of TFA derived from the STOCH-HFO simulation is found to be 0.78 Gg in STOCH-HFO-HY and 0.54 Gg in STOCHEM-HFO-LY. The atmospheric lifetime of TFA is found to be 3.8 days which is close to that in the WMO Ozone Assessment Report (5 days).[64]

3.3 TFA surface distribution

The TFA surface seasonal distribution plots shows high mixing ratios in northern mid-latitudes, with up to 2 ppt for STOCH-HFO-HY (Fig. 3a) and 1.5 ppt for STOCH-HFO-LY (Fig. 3c) in European countries (*e.g.* France, Austria, Italy), 0.7 ppt for STOCH-HFO-HY (Fig. 3a) and 0.5 ppt for STOCH-HFO-LY (Fig. 3c) in Northeast United States (*e.g.* New York, Philadelphia, Maryland, Los Angeles), and 0.7 ppt for STOCH-HFO-HY (Fig. 3a) and 0.5 ppt for STOCH-HFO-LY (Fig. 3c) in Asia (*e.g.* China) during June-July-August. Lower abundances of TFA of up to 0.5 ppt (Fig. 3b) and 0.3 ppt (Fig. 3d) in Europe and Asia for STOCH-HFO-HY and STOCH-HFO-LY, respectively and 0.3 ppt (Fig. 3b) in North America for STOCH-HFO-HY are seen during December-January-February. The maximum TFA mixing ratios produced from the oxidation of individual HFO in the grid cell are extracted and investigated in terms of their monthly variations. The monthly variations of maximum TFA mixing ratios (fixed grid cell) showed higher abundances during June-July-August and lower abundances during December-January-February (Fig. S2). The seasonal surface distribution of TFA is driven by the location of HFO emissions (see Fig. S3), the abundances of oxidants (OH, O_3), to react with HFOs converting into TFA and TFA deposition (wet and dry) to remove TFA from the atmosphere. The seasonal variation in these factors leads to seasonal fluctuations in atmospheric TFA mixing ratios. HFO emissions in the model are predominantly distributed over North America, Central Europe, and East Asia. Central Europe and North America have significant markets for HFOs, specifically for HFO-1234yf, which are used in foam blowing and refrigeration applications.[65] Because of their advanced industrial and technological sectors, large populations and developed economies, Tokyo in Japan, South Korea and central-eastern China are also important sources of HFO emissions.[28] The photochemistry between 30° N and 60° N is more rapid during summer than in winter, resulting in high abundance of oxidants, thus the production of TFA through the oxidation of HFOs increases over the polluted regions of the northern hemisphere. Higher gas-phase TFA concentrations during northern hemisphere summer are measured at Beijing, China[66–68] and Ontario, Canada[27,69] compared with northern hemisphere winter. The emission fluxes of HFO-1234yf in Asia (2.7 Gg year^{-1}), North America (2.7 Gg year^{-1}) and Europe (4.0 Gg year^{-1}) used in this study are lower than the study of Wang *et al.*[28] by a factor of 16, 9 and 5, respectively, which resulted in the annual surface mixing ratios of TFA of up to 0.07, 0.05, and 0.15 ppt in Asia, North America, and Europe (Fig. 3), a factor of 7-, 7- and 3-fold lower than the study of Wang *et al.*,[28] respectively.

To investigate the formation and dispersion of TFA from fifteen different HFOs, TFA concentration surface distribution plots were generated from the results of the individual STOCH-HFO runs (Fig. 4). The longer lived HFOs (*e.g.* HFO-1336mzzE, HFO-1438ezy, HCFO-1233zdE) travel considerable distances, resulting in more geographically widespread TFA formation with lower concentrations. In contrast, the shorter lived HFOs (*e.g.* HFO-1234yf, HFO-1225yeE, HFO-1225yeZ, HFO-1234zeZ, HCFO-1233xf, HFO-1243zf, HFO-1216) break down more rapidly closer to their emission sources, resulting in more concentrated (elevated) TFA surface levels.

3.4 Atmospheric TFA model-measurement comparison

The atmospheric TFA concentrations from STOCH-HFO-HY, STOCH-HFO-LY, STOCH-HFO-HY-1, STOCH-HFO-LY-1 STOCH-HFO-HY-100 and STOCH-HFO-LY-100 model simulations were compared with measurement data. As shown in Table 4, the modelled TFA derived from 10 Gg year^{-1} HFO emissions are more consistent with measurements than that of TFA derived from 1 and 100 Gg year^{-1} HFO emissions.

Transition from HFCs to HFOs resulted from the Kigali Amendment to the Montreal Protocol which came into force in 2019 and required a phase down in HFCs production and use. The

Table 4 Comparison of modelled and measured atmospheric TFA concentrations at different surface locations[a]

			Model TFA (ppt)			
Location	Time	Measured TFA (ppt)	1 Gg	10 Gg	100 Gg	References
Toronto, Canada	Feb–Apr 2022	<LOD-0.979	0.02–0.02	0.17–0.23	1.72–2.33	Young *et al.*[27]
	Jun–Aug 2022	<LOD-1.72	0.05–0.06	0.45–0.61	4.48–6.10	
Toronto, Canada	Sep–Oct 2021	0.10	0.02–0.03	0.24–0.33	2.43–3.27	Ye *et al.*[70]
Toronto, Canada	Jun–Dec 2000	0.07–1.16	0.03–0.04	0.28–0.38	2.82–3.83	Martin *et al.*[69]
Guelph, Canada	Jan–Dec 2000	0.06–0.41	0.02–0.03	0.23–0.31	2.29–3.11	Martin *et al.*[69]
Reno, US	Sep–Oct 1994	0.34–0.71	0.02–0.03	0.16–0.25	1.62–2.53	Zehavi & Seiber[71]
New Jersey, US	Jul–Aug 2023	0.44–0.77	0.04–0.06	0.42–0.57	4.21–5.73	Mattila & Offenberg[72]
Beijing, China	Apr–Oct 2012	0.43 ± 0.29	0.05–0.07	0.47–0.65	4.71–6.48	Hu *et al.*[66]
Beijing, China	May 2012–Apr 2013	0.29 ± 0.11	0.04–0.05	0.38–0.52	3.77–5.16	Wu *et al.*[67]
Beijing, China	Apr 2013–Apr 2016	0.29 ± 0.04	0.04–0.06	0.42–0.58	4.24–5.81	Zhang *et al.*[68]

[a] Note: measurement LODs in the study by Young *et al.*[27] range from 0.010–0.341 and 0.039–0.407 ppt for Feb–Apr 2022 and Jun–Aug 2022, respectively. The range of model TFA are derived from STOCH-HFO-LY (lower end) and STOCH-HFO-HY (upper end) with different emission scenarios (1 Gg, 10 Gg and 100 Gg year^{-1})

model considered only HFO emissions and did not include HFC emissions (HFCs can act as TFA precursors, but with much lower yields compared with HFOs);[15] hence, the model is not relevant to measurement data for TFA before 2019. Most of the observational data in Table 4 were obtained during periods when HFOs were not yet used and the observed TFA must have come from sources other than HFOs.

3.5 Deposition of TFA

Atmospheric TFA is deposited into the global aquatic and terrestrial environment.[73] Fig. 5 shows our calculated annual and seasonal TFA surface depositions over land and the oceans from both dry and wet deposition. The model predicts that North America (up to 0.5×10^{-3} Mg km^{-2} years^{-1}), Europe (up to 1.0×10^{-3} Mg km^{-2} years^{-1}), and Asia (up to 1.0×10^{-3} Mg km^{-2} years^{-1}) are hot spots for deposition of TFA from HFO degradation, as supported by the distribution plots of atmospheric TFA mixing ratios in Fig. 3. The hot spots for TFA deposition are associated with high levels of industrial activity, especially where refrigeration and air conditioning systems are prevalent. Additionally, the three identified hot spots for TFA deposition are urbanised regions with high population densities. This outcome agrees with the study of Freeling *et al.*[73] who found the highest TFA wet deposition fluxes were located in densely populated regions of Germany. Furthermore, Chen *et al.*[75] concluded that refrigerant emissions correlate positively with regions with high degrees of urbanisation and large numbers of private vehicles, thus resulting in higher levels of TFA in precipitation, in turn increasing the wet deposition of TFA. However, a significant proportion of TFA was found to be deposited outside the emission regions, consistent with the studies of David *et al.*[17] and Wang *et al.*[74]

Fig. 5b and c show that TFA deposition during winter are generally distributed over larger areas than in summer. This

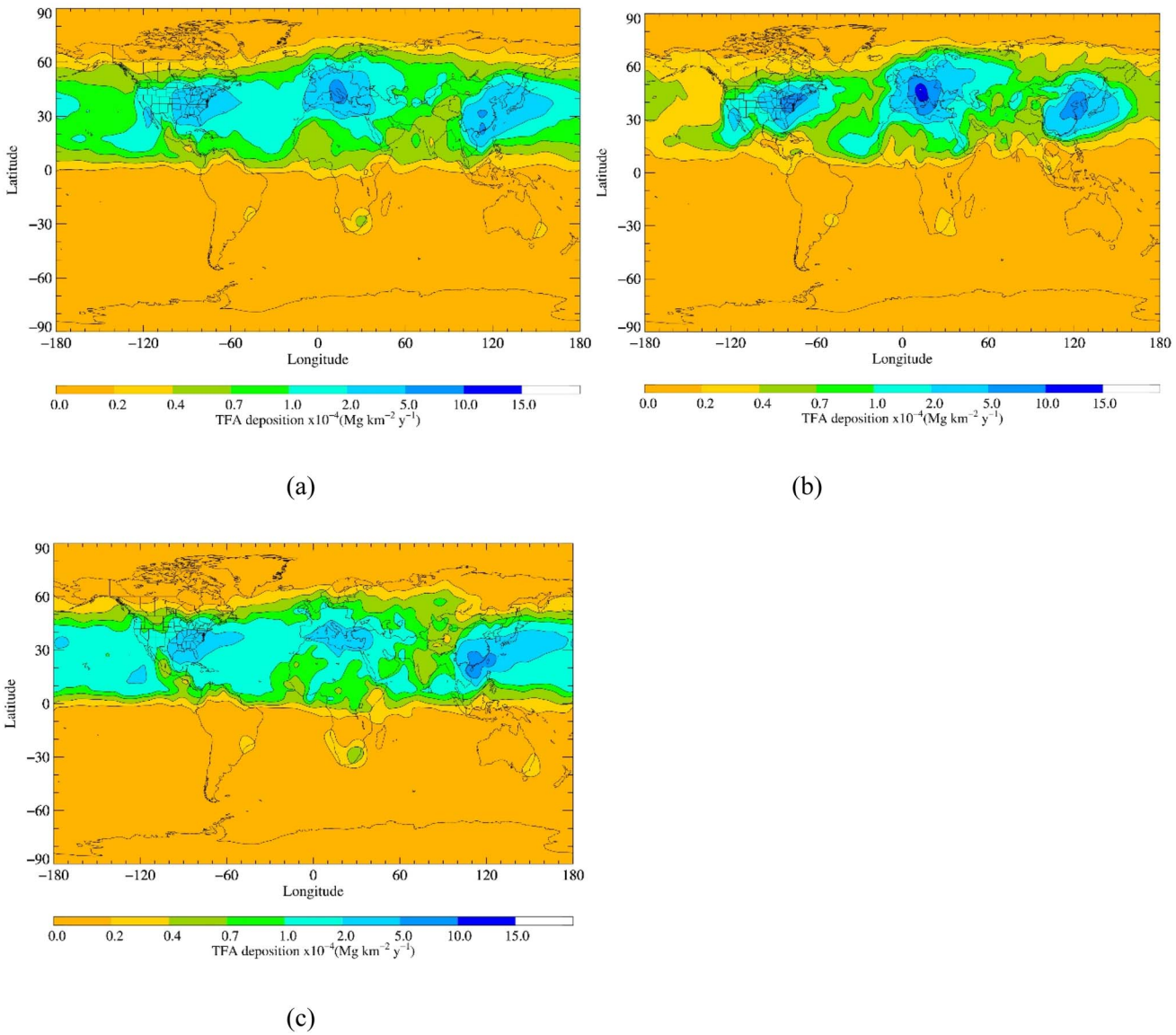

Fig. 5 Surface distribution plots of TFA deposition simulated by the STOCH-HFO-HY, (a) annual, (b) June-July-August, (c) December-January-February. Similar plots for STOCH-HFO-LY scenario can be found in SI (Fig. S5).

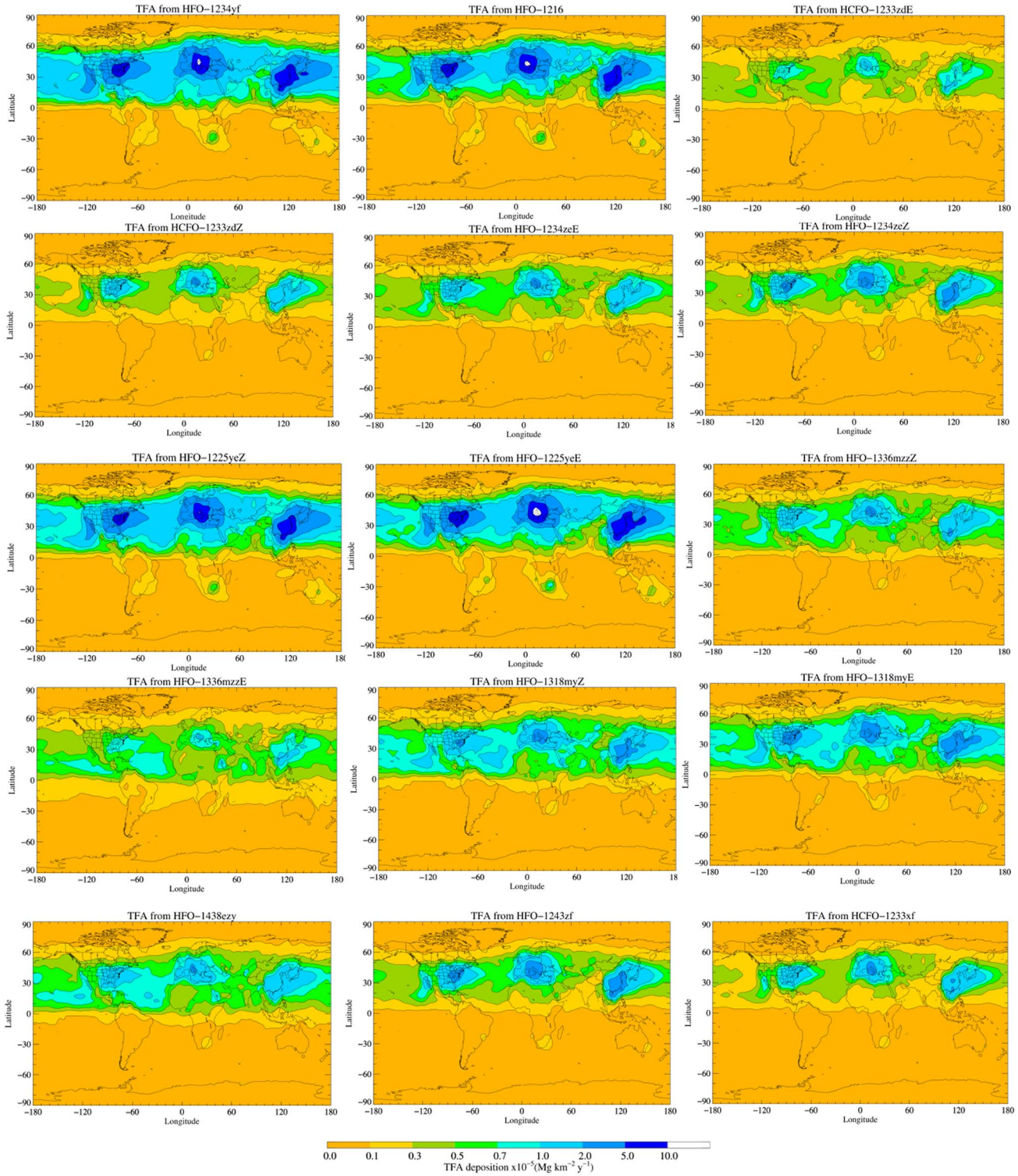

Fig. 6 Annual surface distribution plots of TFA deposition produced from individual HFO oxidations with high TFA yields. The annual surface distribution plots of TFA deposition produced from eight HFOs with lower TFA yields can be found in the SI (Fig. S6).

reflects the lower photochemical activity and longer atmospheric lifetimes of the HFOs in winter.

We compared the TFA deposition surface plots from the results of the individual STOCH-HFO simulations to assess the spatial variations in their TFA depositions (Fig. 6). The deposition of TFA from shorter-lived HFOs, *e.g.* HFO-1216, HFO-1234yf, HFO-1225yeE, HFO-1225yeZ, HFO-1243zf, HCFO-1233xf, HFO-1234zeZ is more concentrated and localised, whereas TFA deposition from longer-lived HFOs, *e.g.* HFO-1336mzzE, is less concentrated and more dispersed. This

difference is because HFO-1336mzzE can travel greater distances once emitted before it oxidizes to TFA, leading to a more widespread deposition. Conversely, HFO-1216, HFO-1234yf, HFO-1225yeE, HFO-1225yeZ, HFO-1243zf, HCFO-1233xf and HFO-1234zeZ oxidize more rapidly, resulting in faster production and deposition of TFA closer to the emission sources, with deposition hotspots located in Central Europe, East Asia, and North America (Fig. 5).

The maximum annual TFA deposition fluxes derived from each HFO are found in either Italy or Austria (Fig. 6). The monthly deposition fluxes analysis shows that the maximum TFA deposition from HFOs follows the trend as: HFO-1234yf (3.1×10^{-4} Mg km^{-2} years^{-1}, Austria) > HFO-1225yeZ (2.9×10^{-4} Mg km^{-2} years^{-1}, Austria) > HFO-1225yeE (2.7×10^{-4} Mg km^{-2} years^{-1}, Italy) > HFO-1216 (2.4×10^{-4} Mg km^{-2} years^{-1}, Italy) > HFO-1243zf (9.6×10^{-5} Mg km^{-2} years^{-1}, Italy) > HCFO-1233xf (5.0×10^{-5} Mg km^{-2} years^{-1}, Italy) > HFO-1234zeZ (9.0×10^{-5} Mg km^{-2} years^{-1}, Italy) > HFO-1318myE (1.2×10^{-4} Mg km^{-2} years^{-1}, Austria) > HFO-1234zeE (6.8×10^{-5} Mg km^{-2} years^{-1}, Italy) > HCFO-1233zdZ (6.1×10^{-5} Mg km^{-2} years^{-1}, Italy) > HFO-1336mzzZ (7.0×10^{-5} Mg km^{-2} years^{-1}, Italy) > HFO-1318myZ (8.0×10^{-5} Mg km^{-2} years^{-1}, Italy) > HFO-1438ezy (5.0×10^{-5} Mg km^{-2} years^{-1}, Italy) > HCFO-1233zdE (3.7×10^{-5} Mg km^{-2} years^{-1}, Italy) > HFO-1336mzzE (3.0×10^{-5} Mg km^{-2} years^{-1}, Italy). The monthly variations of these maximum depositions (fixed grids) show maximum during northern summer months (Jun-Jul-Aug), and minimum deposition during the northern winter months (Dec-Jan-Feb) (Fig. 7). These findings are consistent with the studies of Freeling *et al.*[73] and Wang *et al.*[74] who demonstrated a significant seasonal pattern in the wet deposition fluxes of TFA across Germany and East Asia, respectively, with maxima during the summer due to higher concentrations of photochemically generated oxidants such as OH radicals.

As is shown in Fig. 8, we analysed the hotspot grid cells using the percentile method (≥95th percentile) and identified 130 hotspots for TFA deposition (43 in Europe, 35 in North America, 52 in Asia). Over these hotspots, the annual average TFA deposition for both STOCH-HFO-HY and STOCH-HFO-LY was found to be greater over the land compared with the ocean for Europe (61% *vs.* 39%). However, the annual TFA depositions were found to be higher over the ocean than the land for Asia (47% *vs.* 53%) and for North America (41% *vs.* 59%). This was determined by intersecting the model grid with land polygons (taken from Natural Earth) to determine the proportion of each grid cell covering landmass or ocean.

During Dec-Jan-Feb months, the identified hotspots are dominated by Asia (58 in Asia, 39 in North America, 28 in Europe for STOCH-HFO-HY and 56 in Asia, 40 in North America, 29 in Europe for STOCH-HFO-LY) and TFA deposition is significant over the ocean rather than the land (North America: 68% *vs.* 32%, Asia: 65% *vs.* 35%, Europe: 42% *vs.* 58%) (see SI Fig. S8). However, during the period June-July-August, the identified hotspots are dominated by Europe (40 in Asia, 32 in North America, 58 in Europe) and Asia (52 in Asia, 43 in Europe and 29 in North America) for STOCH-HFO-HY and STOCH-HFO-LY, respectively. TFA deposition during June-July-August is predominantly over the land rather than the ocean for all regions (North America: 52% *vs.* 48%, Asia: 61% *vs.* 39%, Europe: 67% *vs.* 33%) (see SI Fig. S8).

Table 5 shows that 46% of all HFO emissions (with a range of 30% for longer-lived HFOs to 57% for shorter-lived HFOs) are deposited as TFA within the emission regions in STOCH-HFO-HY, while the remaining fractions are distributed toward the ocean and other continents. The hotspot grid cells analysis shows that TFA deposition from all HFOs dominates in the ocean (56%) compared with land (44%) (Table 5). A variable amount of TFA deposition from individual HFOs are found over land (with a range of 34% to 50%) and the ocean (50 to 66%) (Table 5).

3.6 Impact of regional emissions

Model simulations with regional emissions (for Europe, North America and Asia) of the longest-lived (HFO-1336mzzmE),

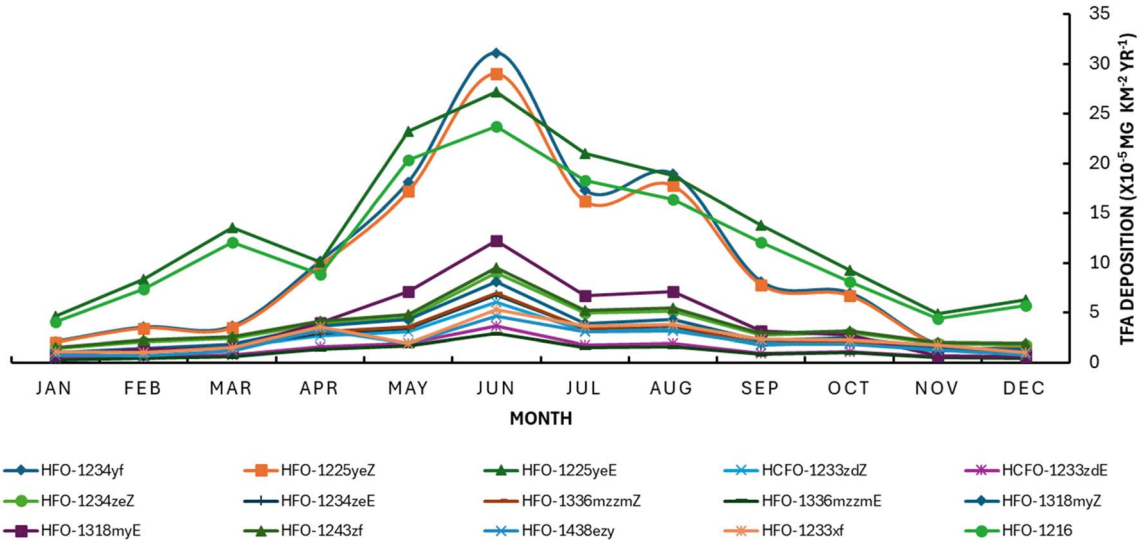

Fig. 7 Monthly variation of maximum TFA deposition flux (fixed grid cell) derived from individual HFO oxidation reactions in the model.

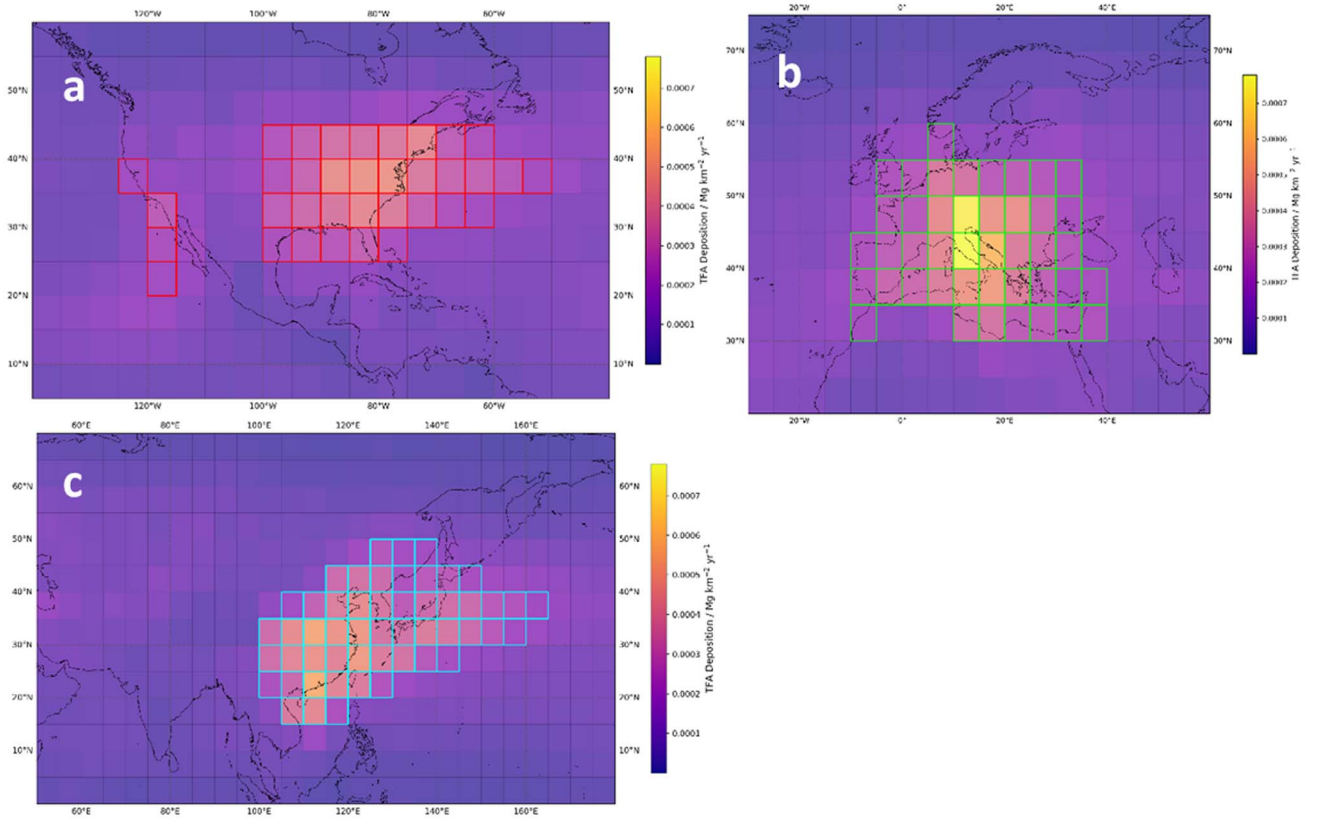

Fig. 8 The hot spots (highlighted, >95th percentile) for TFA deposition flux per grid box simulated by the STOCH-HFO-HY model (a) North America (b) Europe, and (c) Asia. Similar figures for STOCH-HFO-HY model simulations can be found in the SI (Fig. S7).

shortest-lived (HFO-1216), and most widely used HFO (HFO-1234yf) were performed to obtain a deeper understanding of the dependence of TFA deposition patterns on the HFO lifetime. Determining how far the TFA deposition travels between continents is also essential for assessing the potential environmental implications of the use of different HFOs.

Fig. 9 displays the ratio of TFA deposition from regional HFO emission from North America, Asia, and Europe to global HFO emission for three selected HFOs: HFO-1234yf, HFO-1216, and HFO-1336mzzE, respectively. Amongst these, HFO-1216 has the highest TFA deposition (80–100%) from local HFO-1216 emissions (Fig. 9d–f) with the remining deposited TFA transporting

Table 5 Percentage of TFA deposition within the emission region, over land and over the ocean[a]

HFO	TFA total deposition (Gg year^{-1})	TFA percentage deposition within the emission regions (%)	TFA deposition over land (%)	TFA deposition over ocean (%)
All HFO	22650 (15730)	46 (47)	44 (45)	56 (55)
HFO-1234yf	3010	49	45	55
HFO-1225yeZ	2610	51	47	53
HFO-1225yeE	2770	56	49	51
HCFO-1233zdZ	770 (60)	47 (45)	45 (44)	55 (56)
HCFO-1233zdE	720 (50)	37 (36)	39 (38)	61 (62)
HFO-1234zeZ	1020 (80)	50 (48)	46 (45)	54 (55)
HFO-1234zeE	960 (70)	44 (42)	43 (42)	57 (58)
HFO-1336mzZ	1150 (80)	40 (39)	41 (40)	59 (60)
HFO-1336mzE	1040 (70)	30 (29)	34 (34)	66 (66)
HFO-1318myZ	1540	39	40	60
HFO-1318myE	1600	43	42	58
HFO-1243zf	1070 (80)	51 (49)	46 (46)	55 (56)
HFO-1438ezy	1280	37	38	62
HCFO-1233xf	800 (60)	51 (49)	46 (46)	54 (54)
HFO-1216	2410	57	50	50

[a] The values are in brackets are produced from the model simulation, STOCH-HFO-LY.

from other continental HFO-1216 emissions. The high local deposition for HFO-1216 is attributed to its short-lived nature, as it rapidly degrades into TFA, resulting in a localised deposition of TFA that does not extend far from the source of emission. A similar deposition pattern, but with slightly reduced deposition (70–100%) from local HFOs emissions, is shown in Fig. 9a–c for HFO-1234yf, and is due to its shorter lifetime. With the North America emission scenario, TFA deposition is found to be maximum in eastern North America (Fig. 9a), which is consistent with the studies of Kazil *et al.*[76] and Luecken *et al.*[15] who showed higher TFA deposition in the eastern United States and downwind of the Los Angeles basin because of strong HFO-1234yf sources in these regions. We found 31%, 32%, and 30% TFA deposition from HFO-1234yf for separate North America, Europe and Asia emission scenarios. These results are consistent with Henne *et al.*[16] who showed ~30–40% TFA deposition within Europe from the European HFC-1234yf emissions, with the remaining fraction distributed toward the Atlantic Ocean, Central Asia, Northern, and Tropical Africa. Our results are also comparable with the study of Wang *et al.*[28] who used the GEOS-Chem model to simulate China, US and Europe emissions of HFO-1234yf and found 55%, 31%, and 31% TFA deposition within these regions. The projected emissions of HFO-1234yf in the EU in 2030 were estimated to be 7.09 Gg.[77] Scaling the data in Fig. 9c by a factor of 1.77 and summing over the Rhine basin gives an estimate for TFA deposition of approximately 55 Mg. This value can be compared to the Rhine discharge flux of TFA in 2023 of approximately 93 Mg.[5]

For the longest lived HFO, HFO-1336mzzE, the TFA deposition is less concentrated and more widespread, having crossed multiple continents (Fig. 9g–i). Around 50–70% of deposited TFA contributing from local HFO-1336mzzE emissions with the remaining deposited TFA transporting from other continental HFO-1336mzzE emission regions.

3.7 TFA deposition potential (TDP) for selected HFOs

TFA Deposition Potential (TDP) of the 15 candidate HFO species was developed using HFO-1234yf as a reference species, giving

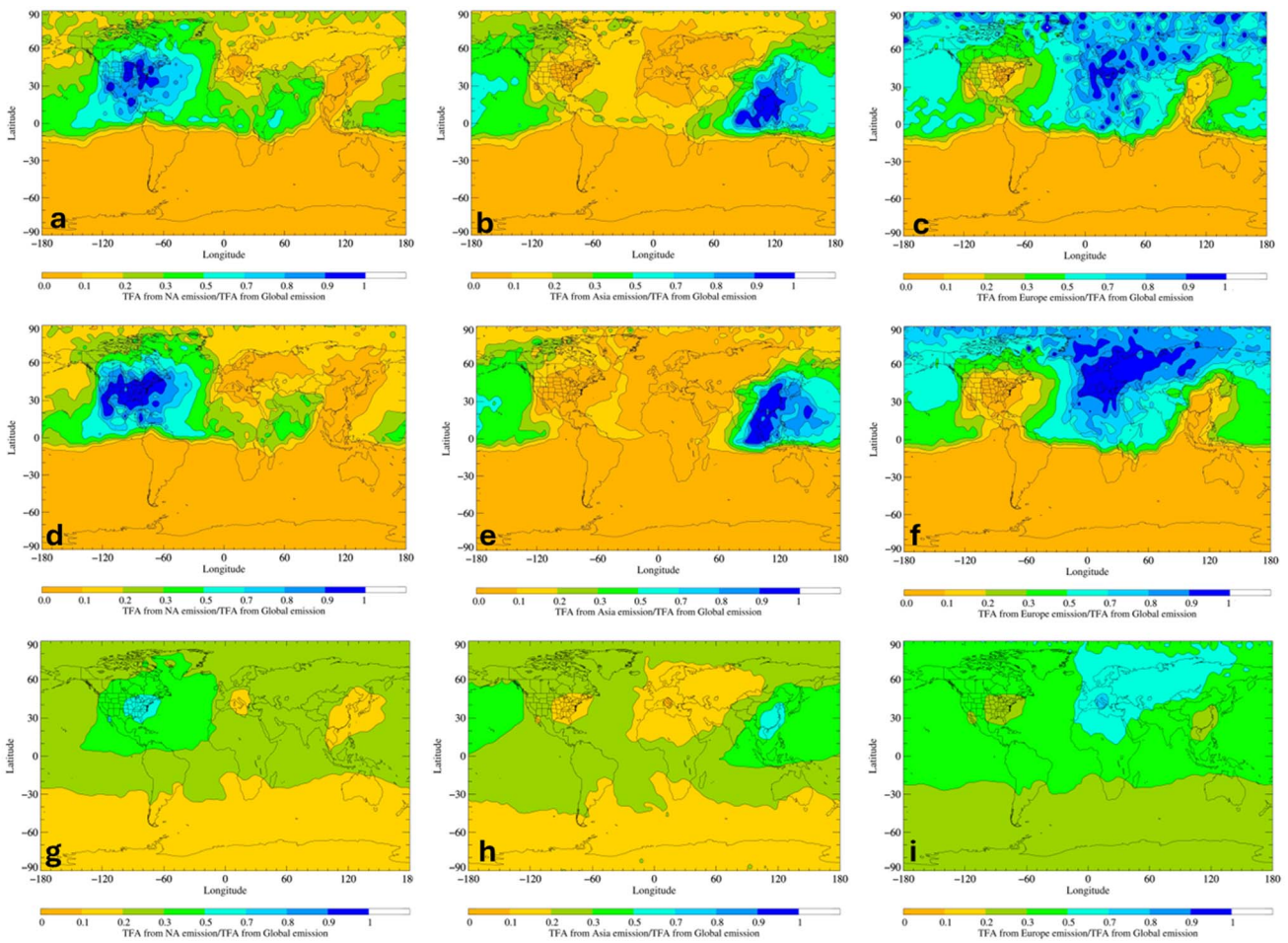

Fig. 9 The ratio of TFA deposition from regional HFO emission to global HFO emission for three selected HFOs. (a)–(c) are derived from North America, Asia and Europe emissions, respectively for the most widely used HFO, HFO-1234yf, (d)–(f) are derived from NA, Asia and Europe emissions, respectively for the short-lived HFO, HFO-1216 and (g)–(i) are derived from North America, Asia and Europe emissions, respectively for the long-lived HFO, HFO-1336mzzE.

Table 6 Maximum TFA concentration, total TFA deposition and TFA deposition potential (TDP) for selected HFOs

HFO Name	TFA maximum concentration (ppt)	TFA annual total deposition (Mg year^{-1})	TDP	TDP1 $k_{HFO+OH}{}^{a}\alpha/k_{HFO\text{-}1234yf+OH}$
HFO-1234yf	0.31	3010.57	1.00	1.00
HFO-1225yeZ	0.29	2614.43	1.08	1.13
HFO-1225yeE	0.41	2769.86	1.44	1.92
HCFO-1233zdZ	0.09 (0.01)	764.94 (56.08)	1.14 (1.04)	0.25 (0.02)
HCFO-1233zdE	0.05 (0.00)	717.71 (51.73)	0.72 (0.67)	0.10 (0.01)
HFO-1234zeZ	0.13 (0.01)	1019.83 (74.69)	1.28 (1.17)	0.36 (0.02)
HFO-1234zeE	0.10 (0.01)	960.54 (70.05)	1.00 (0.92)	0.19 (0.01)
HFO-1336mzzZ	0.10 (0.01)	1148.57 (83.66)	0.85 (0.78)	0.26 (0.02)
HFO-1336mzzE	0.04 (0.00)	1042.80 (74.13)	0.40 (0.37)	0.06 (0.004)
HFO-1318myZ	0.12	1538.98	0.74	0.34
HFO-1318myE	0.12	1595.61	0.74	0.52
HFO-1243zf	0.14 (0.01)	1073.51 (78.71)	1.29 (1.13)	0.36 (0.02)
HFO-1438ezy	0.07	1276.36	0.49	0.01
HCFO-1233xf	0.08 (0.01)	797.02 (59.73)	0.94 (0.78)	0.35 (0.02)
HFO-1216	0.36	2412.38	1.44	1.87

[a] Note: TDP1 were calculated using TFA yields (α) from HFO + OH reactions shown in SI Table S1. The values in the brackets are calculated when the TFA yields from HFO + OH reactions are in lower limit.

measure of the peak TFA deposition from the candidate species relative to that of the reference species (TDP = total TFA deposition per maximum surface concentration by a HFO/total TFA deposition per maximum surface concentration by HFO-1234yf). Table 6 presents the TDPs for the 15 HFOs used in this investigation. Of these, HFO-1225yeE, HFO-1243zf, HFO-1216, HCFO-1233zdZ, HFO-1225yeZ and HCFO-1234zeZ have the highest TFA deposition (TDP > 1.0) relative to HFO-1234yf, and HFO-1336mzzE and HFO-1438ezyE have the lowest level of peak TFA deposition (TDP < 0.5). The studied HFOs can be ranked in terms of their increasing TDP as: HFO-1336mzzE < HFO-1438ezy < HCFO-1233zdE < HFO-1318myE < HFO-1318myZ < HFO-1336mzzZ < HCFO-1233xf < HFO-1234zeE < HFO-1234yf < HFO-1225yeZ < HCFO-1233zdZ < HFO-1234zeZ < HFO-1243zf < HFO-1225yeE < HFO-1216. In a simplest way, we calculated the TDP1 using the kinetic data of k_{HFO+OH} (Table 1) and the yields of TFA from the reaction of HFO + OH (Table S1). Except HFO-1234zeE, HFO-1318myE, HFO-1243zf, HFO-1234zeZ and HCFO-1233zdZ, the ranking of other 10 HFOs in terms of TDP1 is consistent with that of TDP (Fig. S9). The use of this TDP metric, which scales with OH lifetime, facilitates a clearer understanding of the environmental consequences of HFO use, offering a framework for more informed decision-making.

4 Conclusion

The atmospheric formation and the surface deposition of TFA in the gas-phase oxidation of HFOs have been investigated using a global chemistry transport model, STOCHEM-CRI. TFA production by OH-initiated oxidation of HFOs (97%) dominates oxidation initiated by O_3 (~3%). In the context of hypothetical emission fluxes (1 Gg year^{-1}, 10 Gg year^{-1} and 100 Gg year^{-1}) and emission distributions (similar to HFC-134a in 2010) for all HFOs, HFO-1225yeZ, HFO-1225yeE, HFO-1216, and HFO-1234yf are found to be the most significant contributors, responsible for up to 44% of the total TFA formation. The highest atmospheric TFA concentrations are predicted to arise in the northern mid-latitudes, with mixing ratios of up to 2 ppt in central Europe during June-July-August, and up to 1 ppt in east Asia during December-January-February. Highest TFA depositions were estimated in three regions: up to 1.0×10^{-3} Mg kg^{-2} years^{-1} in Europe, up to 0.5×10^{-3} Mg kg^{-2} years^{-1} in North America, and up to 1.0×10^{-3} Mg kg^{-2} years^{-1} in Asia. 46% of HFO emissions are deposited as TFA within the emission regions, and significant amounts (56%) of TFA deposition occur over the oceans. The seasonal variations of atmospheric TFA concentration and TFA deposition are highest during the summer and lowest during the winter. TFA deposition from longer-lived HFOs (*e.g.* HFO-1336mzzE) is less concentrated and more dispersed than from shorter-lived HFOs (*e.g.* HFO-1216). The regional emission scenarios show that the shorter-lived HFOs rapidly degrade into TFA, resulting in localised deposition (predominantly in Europe, North America and Asia) of TFA that does not extend far from the source of emission. Although TFA deposition is less concentrated with the use of longer-lived HFO-1336mzzE, it nonetheless spreads across multiple regions. HFO-1225yeE, HFO-1243zf, HFO-1216, HCFO-1233zdZ, HFO-1225yeZ and HCFO-1234zeZ are associated with elevated levels of TFA deposition, quantified by a newly defined TFA Deposition Potential (TDP) metric with TDP > 1. The present work quantities the spatial distribution of TFA deposition following release of 15 different HFOs. Further work is needed to quantify other anthropogenic TFA sources such as from the degradation of pesticides and pharmaceuticals and continued monitoring of TFA levels in rain, river, lake, and sea water are needed to improve our understanding of the sources of TFA in the environment.

Conflicts of interest

There are no conflicts to declare.

Data availability

The data presented in this study are available on request from the corresponding authors.

Supplementary information: kinetic studies of the reaction of OH radicals and O_3 with HFOs studied. Kinetic data for the reaction between the HFO and OH radicals and O_3 (Section 1). Lifetime, GWP and TFA yields (Section 2). Estimated lifetimes for HFOs and TFA yields (Table S1). Details of each HFO oxidation simulation (Table S2). The scematic diagram of the oxidation of HFO by OH and O_3 producing TFA (Fig. S1). Monthly variation of maximum TFA mixing ratios produced from the individual HFO oxidation reactions in the model (Fig. S2). Annual HFO emission distribution adapted from 2010 HFC-134a EDGAR emission inventory (Fig. S3). Annual surface distribution plots of TFA mixing ratios produced from eight HFOs with lower TFA yields (Fig. S4). Surface distribution plots of TFA deposition simulated by the STOCH-HFO-LY, (a) annual, (b) June–July–August, (c) December–January–February (Fig. S5). Annual surface distribution plots of TFA depositions produced from eight HFOs with lower TFA yields (Fig. S6). The hot spots for TFA deposition flux per grid box simulated by the STOCH-HFO-LY model (a) North America (b) Europe, and (c) Asia (Fig. S7). The hot spots of TFA deposition flux during June–July–August (a) December–January–February (b) simulated by the STOCH-HFO-HY, the hot spots of TFA deposition flux during June–July–August (c) December–January–February (d) simulated by the STOCH-HFO-LY (Fig. S8). Comparative TFA deposition potential from the model study (TDP) and simple kinetic study (TDP1) (Fig. S9). See DOI: https://doi.org/10.1039/d5ea00108k.

Acknowledgements

We thank various NERC grants (NE/K004905/1; NE/J009008/1; NE/I014381/1, NE/G01972X/1, NE/X00452X/1, NER/A/S/2001/00438, NER/A/S/2001/00374), Bristol ChemLabS and the Primary Science Teaching Trust under whose auspices various aspects of this work were carried out. C. J. P.'s work was carried out at Jet Propulsion Laboratory, California Institute of Technology, under contract with the National Aeronautics and Space Administration (NASA, 80NM0018D0004) and was supported by the Upper Atmosphere Research and Tropospheric Chemistry Programs.

References

1 H.-P. H. Arp, A. Gredelj, J. Glüge, M. Scheringer and I. T. Cousins, The global threat from the irreversible accumulation of Trifluoroacetic Acid (TFA), *Environ. Sci. Technol.*, 2024, **58**, 19925–19935.
2 M. d. l. A. Garavagno, R. Holland, M. A. H. Khan, A. J. Orr-Ewing and D. E. Shallcross, Trifluoroacetic acid: Toxicity, Sources, Sinks and future prospects, *Sustainability*, 2024, **16**, 2382.
3 H. A. Frank, A. Klein and D. Renschen, Environmental trifluoroacetate, *Nature*, 1996, **382**, 34.
4 B. Scott, R. Macdonald, K. Kannan, A. Fisk, A. Witter, N. Yamashita, L. Durham, C. Spencer and D. Muir, Trifluoroacetate profiles in the Arctic, Atlantic, and Pacific Oceans, *Environ. Sci. Technol.*, 2005, **39**, 6555–6560.
5 P. J. Neale, S. Hylander, A. T. Banaszak, *et al.*, Environmental consequences of interacting effects of changes in stratospheric ozone, ultraviolet radiation, and climate: UNEP Environmental Effects Assessment Panel, Update 2024, *Photochem. Photobiol. Sci.*, 2025, **24**, 357–392.
6 S. Madronich, B. Sulzberger, J. D. Longstreth, T. Schikowski, M. P. S. Andersen, K. R. Solomon and S. R. Wilson, Changes in tropospheric air quality related to the protection of stratospheric ozone in a changing climate, *Photochem. Photobiol. Sci.*, 2023, **22**, 1129–1176.
7 T. L. Bott and L. J. Standley, Incorporation of trifluoroacetate, a hydrofluorocarbon decomposition byproduct, by freshwater benthic microbial communities, *Water Res.*, 1999, **33**, 1538–1544.
8 L. Zhang, H. Sun, Q. Wang, H. Chen, Y. Yao, Z. Zhao and A. C. Alder, Uptake mechanisms of perfluoroalkyl acids with different carbon chain lengths (C2-C8) by wheat (Triticum Acstivnm L.), *Sci. Total Environ.*, 2019, **654**, 19–27.
9 B. Xu, R. Alizray, D. R. Lammel, S. Riedel and M. C. Rillig, Concentration-dependent response of solid parameters and functions to trifluoroacetic acid, *Eur. J. Soil Sci.*, 2022, **73**, e13266.
10 L. M. Persson, M. Breitholtz, I. T. Cousins, C. A. De Wit, M. MacLeod and M. S. McLachlan, Confronting unknown planetary boundary threats from Chemical pollution, *Environ, Sci. Technol.*, 2013, **47**, 12619–12622.
11 M. L. Hanson, S. Madronich, K. Solomon, M. P. Sulbaek Andersen and T. J. Wallington, Trifluoracetic acid in the Environment: Consensus, gaps and next steps, *Environ. Toxicol. Chem.*, 2024, **43**, 2091–2093.
12 T. J. Wallington, W. F. Schneider, D. R. Worsnop, O. J. Nielsen, J. Sehested, W. J. Debruyn and J. A. Shorter, The environmental impact of CFC replacements HFCs and HCFCs, *Environ. Sci. Technol.*, 1994, **28**, 320A–326A.
13 R. Holland, M. A. H. Khan, I. Driscoll, R. Chhantyal-Pun, R. G. Derwent, C. A. Taatjes, A. J. Orr-Ewing, C. J. Percival and D. E. Shallcross, Investigation of the production of Trifluoracetic acid from two halocarbons, HFC-134a and HFO-1234yf and its fates using a global three-dimensional chemical transport model, *ACS Earth Space Chem.*, 2021, **5**, 849–857.
14 D. Fahey, P. A. Newman, J. A. Pyle, B. Safari and M. P. Chipperfield, *et al.*, *Scientific Assessment of Ozone Depletion: 2018, Global Ozone Research and Monitoring Project-Report No. 58*, World Meteorological Organization, 2018, 588, 978.
15 D. J. Luecken, R. L. Waterland, S. Papasavva, K. N. Taddonio, W. T. Hutzell, J. P. Rugh and S. O. Andersen, Ozone and TFA impacts in North America from degradation of 2,3,3,3-tetrafluoropropene (HFO- 1234yf), a potential greenhouse gas replacement, *Environ. Sci. Technol.*, 2010, **44**, 343–348.
16 S. Henne, D. E. Shallcross, S. Reimann, P. Xiao, D. Brunner, S. O'Doherty and B. Buchmann, Future emissions and

atmospheric fate of HFC-1234yf from mobile air conditioners in Europe, *Environ. Sci. Tecnol.*, 2012, **46**, 1650–1658.

17 L. M. David, M. Barth, L. Höglund-Isaksson, P. Purohit, G. J. Velders, S. Glaser and A. R. Ravishankara, Trifluoroacetic acid deposition from emissions of HFO-1234yf in India, China, and the Middle East, *Atmos. Chem. Phys.*, 2021, **21**, 14833–14849.

18 G. Y. Xie, J. N. Cui, Z. H. Zhai and J. B. Zhang, Distribution characteristics of trifluoroacetic acid in the environments surrounding fluorochemical production plants in Jinan, China, *Environ. Sci. Pollut. Res.*, 2020, **27**, 983–991.

19 M. S. Zhao, Y. M. Yao, X. Y. Dong, M. Baqar, B. Fang, H. Chen and H. W. Sun, Nontarget Identification of Novel Per- and Polyfluoroalkyl Substances (PFAS) in Soils from an Oil Refinery in Southwestern China: A Combined Approach with TOP Assay, *Environ. Sci. Technol.*, 2023, **57**, 20194–20205.

20 B. Wang, Y. Yao, Y. Wang, H. Chen and H. Sun, Per- and Polyfluoroalkyl Substances in Outdoor and Indoor Dust from Mainland China: Contributions of Unknown Precursors and Implications for Human Exposure, *Environ. Sci. Technol.*, 2022, **56**, 6036–6045.

21 D. A. Ellis, J. W. Martin, A. O. De Silva, S. A. Mabury, M. D. Hurley, M. P. Sulbaek Andersen and T. J. Wallington, Degradation of Fluorotelomer Alcohols: A Likely Atmospheric Source of Perfluorinated Carboxylic Acids, *Environ. Sci. Technol.*, 2004, **38**, 3316–3321.

22 M. K. Vollmer, S. Reimann, M. Hill and D. Brunner, First observation of the Fourth generation synthetic halocarbons HFC-1234yf, HFC-1234ze(E), and HCFC-1233zd(E) in the atmosphere, *Environ. Sci. Technol.*, 2015, **49**, 2703–2708.

23 D. Rust, I. Katharopoulos, M. K. Vollmer, S. Henne, S. O'Doherty, D. Say, L. Emmenegger, R. Zenobi and S. Reimann, Swiss halocarbon emissions from 2019 to 2020 assessed from regional observations, *Atmos. Chem. Phys.*, 2022, **22**, 2447–2466.

24 D. Rust, M. K. Vollmer, S. Henne, T. Buhlmann, A. Frumau, P. van der Bulk, L. Emmenegger, R. Zenobi and S. Reimann, First atmospheric measurements and emission estimates of HFO-1336mzz(Z), *Environ. Sci. Technol.*, 2023, **57**, 11903–11912.

25 M. R. McGillen, Z. T. P. Fried, M. A. H. Khan, K. T. Kuwata, C. M. Martin, S. O'Doherty, F. Pecere, D. E. Shallcross, K. M. Stanley and K. X. Zhang, Ozonolysis can produce longlived greenhouse gases from commercial refrigerant, *Proc. Nat. Academy Sci.*, 2023, **120**, e2312714120.

26 G. Salierno, On the chemical pathways influencing the effective global warming potential of commercial Hydrofluoroolefin gases, *ChemSusChem*, 2024, 1–20.

27 C. J. Young, S. Joudan, Y. Tao, J. J. B. Wentzell and J. Liggio, High time resolution ambient observations of gas-phase perfluoroalkyl carboxylic acids: Implications for atmospheric sources, *Environ. Sci. Technol.*, 2024, **11**, 1348–1354.

28 Z. Wang, Y. Wang, J. Li, S. Henne, B. Zhang, J. Hu and J. Zhang, Impacts of the Degradation of 2,3,3,3-Tetrafluoropropene into Trifluoroacetic Acid from Its Application in Automobile Air Conditioners in China, the United States and Europe, *Environ. Sci. Technol.*, 2018, **52**, 2819–2826.

29 R. Holland, M. A. H. Khan, I. Driscoll, R. Chhantyal-Pun, A. J. Orr-Ewing, C. J. Percival, C. A. Taatjes and D. E. Shallcross, Investigating the atmospheric sources and sinks of Perfluorooctanoic acid using a global chemistry transport model, *Atmosphere*, 2020, **11**, 407.

30 D. S. Stevenson, W. J. Collins, C. E. Johnson and R. G. Derwent, Intercomparison and evaluation of atmospheric transport in a Lagrangian model (STOCHEM), and an Eulerian model (UM), using ^{222}Rn as a short-lived tracer, *Q. J. R. Meteorol. Soc.*, 1998, **124**, 2477–2492.

31 T. C. Johns, R. E. Carnell, J. F. Crossley, J. M. Gregory, J. F. Mitchell, C. A. Senior, S. F. Tett and R. A. Wood, The second Hadley Centre coupled ocean-atmosphere GCM: model description, spinup and validation, *Clim. Dyn.*, 1997, **13**, 103–134.

32 W. J. Collins, D. S. Stevenson, C. E. Johnson and R. G. Derwent, Tropospheric ozone in a global-scale three-dimensional Lagrangian model and its response to NO_x emission controls, *J. Atmos. Chem.*, 1997, **26**, 223–274.

33 M. E. Jenkin, L. A. Watson, S. R. Utembe and D. E. Shallcross, A Common Representative Intermediates (CRI) mechanism for VOC degradation. Part 1: Gas phase mechanism development, *Atmos. Environ.*, 2008, **42**, 7185–7195.

34 L. A. Watson, D. E. Shallcross, S. R. Utembe and M. E. Jenkin, A Common Representative Intermediate (CRI) mechanism for VOC degradation. Part 2: gas phase mechanism reduction, *Atmos. Environ.*, 2008, **42**, 7196–7204.

35 S. R. Utembe, L. A. Watson, D. E. Shallcross and M. E. Jenkin, A Common Representative Intermediates (CRI) mechanism for VOC degradation. Part 3: Development of a secondary organic aerosol module, *Atmos. Environ.*, 2009, **43**, 1982–1990.

36 S. R. Utembe, M. C. Cooke, A. T. Archibald, M. E. Jenkin, D. E. Derwent and D. E. Shallcross, Using a reduced Common Representative Intermediates (CRIv2-R5) mechanism to simulate tropospheric ozone in a 3-D Lagrangian chemistry transport model, *Atmos. Environ.*, 2010, **44**, 1609–1622.

37 M. E. Jenkin, M. A. H. Khan, D. E. Shallcross, R. Bergström, D. Simpson, K. L. C. Murphy and A. R. Rickard, The CRI v2.2 reduced degradation scheme for isoprene, *Atmos. Environ.*, 2019, **212**, 172–182.

38 V. C. Papadimitriou, R. K. Talukdar, R. W. Portmann, A. R. Ravishankara and J. B. Burkholder, CF_3CFCH_2 and (Z)-CF_3CFCHF: temperature dependent OH rate coefficients and global warming potentials, *Phys. Chem. Chem. Phys.*, 2008, **10**, 808–820.

39 O. J. Nielsen, M. S. Javadi, M. P. Sulbaek Andersen, M. D. Hurley, T. J. Wallington and R. Singh, Atmospheric chemistry of $CF_3CF{=}CH_2$: Kinetics and mechanisms of

gas-phase reactions with Cl atoms, OH radicals, and O_3, *Chem. Phys. Lett.*, 2007, **439**, 18–22.

40 M. D. Hurley, J. C. Ball and T. J. Wallington, Atmospheric Chemistry of the Z and E isomers of $CF_3CF{=}CHF$; Kinetics, mechanisms and products of gas-phase reactions with Cl atoms, OH radicals and O_3, *J. Phys. Chem. A*, 2007, **111**, 9789–9795.

41 T. Gierczak, M. Baasandorj and J. B. Burkholder, OH + (E)- and (Z)-1-Chloro-3,3,3-trifluoropropene-1 ($CF_3CH{=}CHCl$) reaction rate coefficients: Stereoisomer-dependent reactivity, *J. Phys. Chem. A*, 2014, **118**, 11015–11025.

42 L. L. Andersen, F. F. Østerstrøm, M. P. S. Andersen, O. J. Nielsen and T. J. Wallington, Atmospheric chemistry of cis-$CF_3CH{=}CHCl$ (HCFO-1233zd(Z)): Kinetics of the gas-phase reactions with Cl atoms, OH radicals and O_3, *Chem. Phys. Lett.*, 2015, **639**, 289–293.

43 M. R. S. Andersen, E. J. K. Nilsson, O. J. Nielsen, M. S. Johnson, M. D. Hurley and T. J. Wallington, Atmospheric chemistry of trans-$CF_3CH{=}CHCl$: Kinetics of the gas-phase reactions with Cl atoms, OH radicals, and O_3, *J. Photochem. Photobiol. A Chem.*, 2008, **199**, 92–97.

44 N. Zhang, L. Chen, J. Mizukado, H. Quan and H. Suda, Rate constants for the gas-phase reactions of (*Z*)-$CF_3CH{=}CHF$ and (*E*)-$CF_3CH{=}CHF$ with OH radicals at 253–328 K, *Chem. Phys. Letts*, 2015, **621**, 78–84.

45 E. J. K. Nilsson, O. J. Nielsen, M. S. Johnson, M. D. Hurley and T. J. Wallington, Atmospheric chemistry of *cis*-$CF_3CH{=}CHF$: Kinetics of reactions with OH radicals and O_3 and products of OH radical initiated oxidation, *Chem. Phys. Lett.*, 2009, **473**, 233–237.

46 V. L. Orkin, L. E. Martynova and A. N. Ilichev, High-Accuracy Measurements of OH Reaction Rate Constants and IR Absorption Spectra: $CH_2{=}CF{-}CF_3$ and *trans*-$CHF{=}CH{-}CF_3$, *J. Phys. Chem. A*, 2010, **114**, 5967–5979.

47 R. Sondergaard, O. J. Nielsen, M. D. Hurley, T. J. Wallington and R. Singh, Atmospheric chemistry of *trans*-$CF_3CH{=}CHF$: Kinetics of the gas-phase reactions with Cl atoms, OH radicals, and O_3, *Chem. Phys. Lett.*, 2007, **443**, 199–204.

48 M. Baasandorj, A. R. Ravishankara and J. B. Burkholder, Atmospheric chemistry of (*Z*)-$CF_3CH{=}CHCF_3$: OH radical reaction rate coefficient and Global Warming Potential, *J. Phys. Chem. A*, 2011, **115**, 10539–10549.

49 F. F. Østerstrøm, S. T. Andersen, T. I. Sølling, O. J. Nielsen and M. P. S. Andersen, Atmospheric chemistry of *Z*- and *E*-$CF_3CHCHCF_3$, *Phys. Chem. Chem. Phys.*, 2017, **19**, 735–750.

50 M. Baasandorj, P. Marshall, R. L. Waterland, A. R. Ravishankara and J. B. Burkholder, Rate coefficient measurements and theoretical analysis of the OH + (*E*)-$CF_3CH{=}CHCF_3$ reaction, *J. Phys. Chem. A*, 2018, **122**, 4635–4646.

51 F. Qing, Q. Guo, L. Chen, H. Quan and J. Mizukado, Atmospheric chemistry of *E*-$CF_3CH{=}CHCF_3$: Reaction kinetics of OH radicals and products of OH-initiated oxidation, *Chem. Phys. Lett.*, 2018, **706**, 93–98.

52 V. L. Orkin, G. A. Poskrebyshev and M. J. Kurylo, Rate constants for the reactions between OH and perfluorinated alkenes, *J. Phys. Chem. A*, 2011, **115**, 6568–6574.

53 S. González, E. Jiménez, B. Ballesteros, E. Martínez and J. Albaladejo, Hydroxyl radical reaction rate coefficients as a function of temperature and IR absorption cross sections for $CF_3CH{=}CH_2$ (HFO-1243zf), potential replacement of CF_3CH_2F (HFC-134a), *Environ. Sci. Pollut. Res.*, 2015, **22**, 4793–4805.

54 A. Soto, B. Ballesteros, E. Jimenez, M. Antinolo, E. Martinez and J. Albaladejo, Kinetic and mechanistic study of the gas-phase reaction of $C_xF_{2x+1}CH{=}CH_2$ (x=1, 2, 3, 4 and 6) with O_3 under atmospheric conditions, *Chemosphere*, 2018, **201**, 318–327.

55 V. C. Papadimitriou and J. B. Burkholder, OH radical reaction rate coefficients, infrared spectrum, and Global Warming Potential of $(CF_3)_2CFCH{=}CHF$ (HFO-1438ezy(*E*)), *J. Phys. Chem. A*, 2016, **120**, 6618–6628.

56 D. K. Thomsen and S. Jørgensen, A theoretical study of the kinetics of OH radical addition to halogen substituted propenes, *Chem. Phys. Letts*, 2009, **481**, 29–33.

57 M. A. Garavagno, A. Wenger, *et al.*, Atmospheric oxidation of hydrofluoroolefins and hydrochlorofluoroolefins by ozone produces HFC-23, PFC-14 and CFC-13, *Environ. Sci. Technol.*, 2025, DOI: 10.1021/acs.est.5c11383.

58 L. Michelat, A. Mellouki, A. R. Ravishankara, H. El Othmani, V. C. Papadimitriou, V. Daële and M. R. McGillen, Temperature-dependent structure-activity relationship of OH + Haloalkene rate coefficients under atmospheric conditions and supporting measurements, *ACS Earth Space Chem.*, 2022, **12**, 3101–3114.

59 K. Tokuhashi, A. Takahashi, M. Kaise, S. Kondo, A. Sekiya and E. Fujimoto, Rate constants for the reactions of OH radicals with $CF_3OCF{=}CF_2$ and $CF_3CF{=}CF_2$, *Chem. Phys. Letts*, 2000, **325**, 189–195.

60 G. Acerboni, J. A. Beukes, N. R. Jensen, J. Hjorth, G. Myhre, C. J. Nielsen and J. K. Sundet, Atmospheric degradation and global warming potentials of three perfluoroalkenes, *Atmos. Environ.*, 2001, **35**, 4113–4123.

61 J. B. Burkholder, S. P. Sander, J. P. D. Abbatt, J. R. Barker, *et al.*, *Chemical Kinetics and Photochemical Data for Use in Atmospheric Studies Evaluation Number 19*, JPL Publication, Pasadena, 2019, 19.

62 T. E. Møgelberg, O. J. Nielsen, J. Sehested, T. J. Wallington and M. D. Hurley, Atmospheric chemistry of CF_3COOH kinetics of the reaction with OH radicals, *Chem. Phys. Lett.*, 1994, **226**, 171–177.

63 T. K. Tromp, M. K. W. Ko, J. M. Rodriguez and N. D. Sze, Potential accumulation of a CFC-replacement degradation product in seasonal wetland, *Nature*, 1995, **376**, 327–330.

64 J. B. Burkholder and O. Hodnebrog, *ANNEX, Summary of Abundances, Lifetimes, ODPs, Res, GWPs and GTPs. Scientific Assessment of Ozone Depletion 2022*, World Meteorological Organisation, Ozone Research and Monitoring- GAW Report No. 278, 2013.

65 C. Booten, S. Nicholson, M. Mann and O. Abdelaziz, *Refrigerants: Market Trends and Supply Chain Assessment, No. NREL/TP-5500-70207*, National Renewable Energy Lab. (NREL), Golden, CO (United States), 2020.

66 X. Hu, J. Wu, Z. H. Zhai, B. Y. Zhang and J. B. Zhang, Determination of Gaseous and Particulate Trifluoroacetic Acid in Atmosphere Environmental Samples by Gas Chromatography-Mass Spectrometry. Fenxi Huaxue, *Chinese J. Anal. Chem.*, 2013, **41**, 1140–1145.

67 J. Wu, J. W. Martin, Z. Zhai, K. Lu, L. Li, X. Fang, H. Jin, J. Hu and J. Zhang, Airborne trifluoroacetic acid its fraction from the degradation of HFC-134a in Beijing, China, *Environ. Sci. Technol.*, 2014, **48**, 3675–3681.

68 B. Zhang, Z. Zhai and J. Zhang, Distribution of trifluoroacetic acid in gas and particulate phases in Beijing from 2013 to 2016, *Sci. Total Environ.*, 2018, **634**, 471–477.

69 J. W. Martin, S. A. Mabury, C. S. Wong, F. Noventa, K. R. Solomon, M. Alaee and D. C. G. Muir, Airborne haloacetic acids, *Environ. Sci. Technol.*, 2003, **37**, 2889–2897.

70 R. X. Ye, R. A. Di Lorenzo, J. T. Clouthier, C. J. Young and T. C. VandenBoer, A Rapid Derivatization for Quantitation of Perfluorinated Carboxylic Acids from Aqueous Matrices by Gas Chromatography-Mass Spectrometry, *Anal. Chem.*, 2023, **95**, 7648–7655.

71 D. Zehavi and J. N. Seiber, An Analytical Method for Trifluoroacetic Acid in Water and Air Samples Using Headspace Gas Chromatographic Determination of the Methyl Ester, *Anal. Chem.*, 1996, **68**, 3450–3459.

72 J. M. Mattila and J. H. Offenberg, Measuring Short-Chain per- and Polyfluoroalkyl Substances in Central New Jersey Air Using Chemical Ionization Mass Spectrometry, *J. Air Waste Manage. Assoc.*, 2024, **74**, 531–539.

73 F. Freeling, D. Behringer, F. Heydel, M. Scheurer, T. A. Ternes and K. Nödler, Trifluoroacetate in precipitation: Deriving a benchmark data set, *Environ. Sci. Technol.*, 2020, **54**, 11210–11219.

74 Y. Wang, L. Liu, X. Qiao, M. Sun, J. Guo, B. Zhao and J. Zhang, Atmospheric fate and impacts of HFO-1234yf from mobile air conditioners in East Asia, *Sci. Total Environ.*, 2024, **916**, 170137.

75 H. Chen, L. Zhang, M. Li, Y. Yao, Z. Zhao, G. Munoz and H. Sun, Per- and polyfluoroalkyl substances (PFASs) in precipitation from mainland China: Contributions of unknown precursors and short-chain (C_2-C_3) perfluoroalkyl carboxylic acids, *Water Res.*, 2019, **153**, 169–177.

76 J. Kazil, S. McKeen, S.-W. Kim, R. Ahmadov, G. A. Grell, R. K. Talukdar and A. R. Ravishankara, Deposition and rainwater concentrations of trifluoroacetic acid in the United States from the use of HFO-1234yf, *J. Geophys. Res. Atmos.*, 2014, **119**(14), 59–14079.

77 K. Zhao, K. Vijayaraghavan, R. Downes, M. Cush, Y. Zhuang, R. Connolly, S. Shi, F. Kristanovich and J. Gupta, *Environmental Modeling of Trifluoroacetic Acid (TFA) Originating from Hydrofluorolefins*, Ramboll, London SE1 8NW, UK, 2023.

